Materials and Design 187 (2020) 108385

Contents lists available at ScienceDirect

Materials and Design

journal homepage: www.elsevier.com/locate/matdes

Effects of defects on mechanical properties in metal additive manufacturing: A review focusing on X-ray tomography insights

Anton du Plessis [a,*], Ina Yadroitsava [b], Igor Yadroitsev [b]

[a] Research group 3D Innovation, Stellenbosch University, Stellenbosch 7602, South Africa
[b] Department of Mechanical and Mechatronics Engineering, Central University of Technology, Bloemfontein 9301, South Africa

HIGHLIGHTS

- Effects of defects on mechanical properties in metal additive manufacturing are reviewed.
- The review focussed on insights from X-ray tomography.
- Not all pores are harmful - smallest pores are harmless.
- Porosity influences both ductility and strength.
- Near-surface pores critical for fatigue properties

GRAPHICAL ABSTRACT

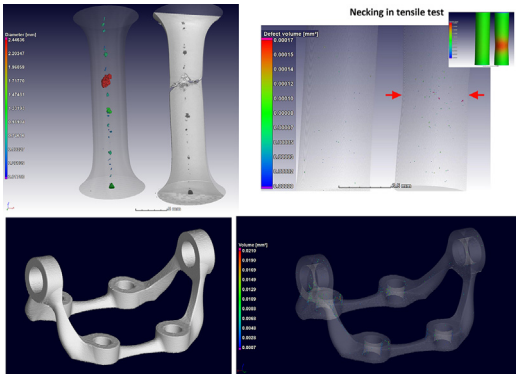

ARTICLE INFO

Article history:
Received 18 July 2019
Received in revised form 28 October 2019
Accepted 22 November 2019
Available online 28 November 2019

Keywords:
X-ray tomography
Laser powder bed fusion
Porosity
Defects
Mechanical properties
Effect of defect

ABSTRACT

X-ray tomography has emerged as a uniquely powerful and non-destructive tool to analyze defects in additive manufacturing. Defects include unintended porosity, rough surfaces and deviations from design, which can have different root causes and can vary significantly among samples. Powder material properties, non-uniform delivery of the powder layer, deformation during manufacturing, deviations from optimal process-parameters caused by changes in the laser beam, the optical components and the scanning system operation, may result in lack of fusion pores, metallurgical pores, keyhole pores, etc. These different types of pores have different typical sizes, shapes and 3D distributions. All types of defects have effects on the mechanical properties of a final part. The use of X-ray tomography to visualize pores in parts (non-destructively) prior to mechanical testing has allowed us to improve our understanding of the effect of this porosity on the mechanical properties of the part (also referred to as "effect of defect"). This can provide the possibility to discriminate critical defects from harmless ones, and thereby build confidence in additive manufacturing processes. This paper reviews the current state of knowledge with regard to the "effect of defect" in metal additive manufacturing, and highlights some relevant examples from our recent work.

* Corresponding author.
E-mail address: anton2@sun.ac.za (A. du Plessis).

https://doi.org/10.1016/j.matdes.2019.108385

Contents

1. Introduction

Additive manufacturing (AM) and especially metal laser powder bed fusion (L-PBF) is a fast growing manufacturing technology allowing excellent mechanical properties for final end-use parts [1–5] in various material types [6], especially for complex geometries and optimized designs which are often impossible to realize by other manufacturing methods [7–9]. The rapid and significant progress in AM over the last decade opens great market potential for L-PBF [10,11]. As AM technology has become better understood, its applications are increasingly being adopted in various industries. Bone replacements by personalised AM implants are now becoming common practice [12,13]. Automotive and aerospace industries have also shown great interest in metal L-PBF components [7,14]. The fabrication of directly printed components with microscale resolution is also of interest to dentistry and jewellery industries [15]. Furthermore, various engineering devices, tools and sensors including heat exchangers and heat sinks for the energy conversion sector is envisioned [16,17]. L-PBF is suitable for in-situ alloyed materials and metal matrix composites and could offer customized functional products for a wide range of engineering applications [18–20]. Additive manufacturing or 3D printing, as a new paradigm of manufacturing, permits the design and production of "metamaterials" with targeted and tunable mechanical, fatigue, acoustic, and even biointegration properties [21]. AM is also able to produce self-transforming structures that can respond to an external input, or so-called '4D printing' of smart materials [22–24].

The presence of manufacturing defects or flaws can have a negative influence on mechanical properties of final produced parts, for all production methods – not only additive manufacturing. Therefore it is important to constantly improve processes and minimize defects which can have such influences. With the emergence of X-ray tomography for inspection of defects in parts, it became possible to inspect final parts and reject them based on defect size or location, according to some criteria. This has become routine for industrial inspection of castings, injection moldings and composites as summarized in the review of industrial applications of X-ray tomography [25]. The use of X-ray tomography has been reviewed for materials sciences [26,27], metrology [28] and additive manufacturing [29,30]. The time and cost benefits of X-ray tomography for screening AM parts was confirmed in recent work [31], where it was convincingly shown that CT scans allow quick investigation of larger material volumes in comparison with destructive and more time-consuming metallographic preparation and analysis.

With the ongoing development of additive manufacturing and L-PBF in particular, it is becoming clear that pores and pore distributions are very complex. Various process parameters, scanning and building strategies, feedstock materials, deformation during manufacturing or other factors lead to a wide range of potential flaws and resulting pore shape and size differences and total volumetric porosity values. The formation of different pore types are discussed in various publications, see for example [32–40]. There is also a wide variety of possible effects of these pores on the mechanical properties, which is not yet fully understood. For example it can be expected that irregular lack of fusion pores are more likely to act as stress concentrators as compared to small near-spherical metallurgical or gas pores, but this has not explicitly been tested due to the only recent emergence of X-ray tomography in "effect of defect" studies, and the difficulty (up to now) in inducing controlled pore distributions.

The reported mechanical properties of metal AM materials vary significantly between studies, especially showing large scatter in fatigue tests [41,42]. A summary of mechanical properties of L-PBF metals is provided in [42,43]. In most publications of L-PBF of metals and reports of their mechanical properties, the focus is usually on relating the microstructure to the mechanical properties and demonstrating the anisotropic microstructure in as-built samples. While microstructure is obviously important, the "effect of defect" is increasingly being acknowledged in recent years and needs to be investigated in more detail as outlined in [41,43]. This is because various defect types may be present in widely varying total content values, maximal sizes, locations and distributions (random vs structured), depending on the production system [1]. Some early L-PBF optimization studies reported at best a density of 87% (13% porosity) [44], with improvements over the years resulting in much higher density and typically achieved densities >99% (<1% porosity) as demonstrated using Archimedes method, analysis of cross-sections by SEM, optical microscopy and X-ray tomography [5,36,45]. It is even possible to generate porosity values as low as 0.002% using optimized process parameters as for example in [46]. This covers a wide range of porosity: from 13% down to 0.002%.

Complex shapes of parts, powder delivery peculiarities, random distribution of powder particles with different sizes and shapes, particle ejection during scanning, fluid flows in the meltpool and unstable formation of single tracks with ripples and humping that forms uneven layers can all lead to the formation of porosity. Even with optimal L-PBF process-parameters, appropriate and verified scanning and building strategies, various errors or imperfections can occur. The probability of pore formation in 3D L-PBF parts cannot be excluded [47], and it is expected that higher porosity will have a stronger effect on mechanical properties.

As was shown in [48–51], hot isostatic pressing (HIP) is a powerful instrument to eliminate porosity and to change the microstructure in AM parts. HIP has a beneficial effect on ductility and fatigue resistance especially for samples with polished/machined surfaces without defects. However, despite the improvements, surface defects are retained

after HIP and this deteriorates the performance properties of AM parts [48,50]. In study [49] it was found that in HIPped electron beam melted titanium parts, pores re-appeared after high temperature annealing (post-HIP) due to the low diffusivity of argon in titanium. In another study, when L-PBF samples were produced in vacuum, HIP with subsequent heat treatments further reduced porosity from 0.095% to 0.067% and 0.044% correspondingly [52]. In this case the porosity did not enlarge due to heat treatment after HIP, due to the pores not containing gas initially. In another study, the formation of alpha-case in Ti alloy occurred with oxygen contamination of the Ar protective atmosphere in which the HIP treatment was conducted and this significantly deteriorated the fatigue properties of cellular L-PBF Ti6Al4V structures [53]. In a recent study [54], HIP treatment was done for complex L-PBF Ti6Al4V cellular structures. Pores in the as-built struts (0.5%) were eliminated by HIP as was shown by CT scans at isotropic voxel size near 20 μm. It was found that HIP also modified the microstructure, improving the ductility and leading to continuous stress-strain curves of the cellular specimens: struts under compression were plastically deformed rather than fracturing layer-wise. Therefore, HIP parameters and their optimization for AM parts as well as post-treatment processes and procedures deserve separate detailed studies. But primarily, optimization of L-PBF process for individual materials is required to minimize defects as far as possible in as-built parts.

X-ray tomography is critical in providing non-destructive insights into porosity values and also on pore distributions. Ideally this can be done prior to mechanical tests to clearly reveal the effect of the defects – relating unexpected premature failures to specific defect types, locations or distributions. Other competing parameters which also influence the mechanical properties are the surface roughness, residual stress and microstructures: the relative importance of each of these in determining the mechanical properties is not always known and can vary between materials. The use of X-ray tomography for inspection and qualification of additively manufactured parts was discussed in detail in [55,56] and the need for more detailed “effect of defect studies” was highlighted in these papers. There are also some limitations to the applicability of CT scans, especially with regard to the resolution limit as was shown in various studies [26,28,29,48,57,58].

The mechanical properties themselves refer to a range of properties, which includes modulus of elasticity, strength (yield strength and ultimate strength), ductility (reduction of area or elongation up to fracture), toughness, hardness, etc. for static/quasi-static loading. For dynamic loading, both high number of cycles to crack initiation and crack growth resistance are desired. For each material type, there typically exists standards for wrought or cast material, which can be taken as a reference to which L-PBF materials must adhere. For example, for Ti6Al4V ELI, the minimum prescribed values for L-PBF are given in [59] with elongation >8%, yield strength >760 MPa. A summary of literature studies of additively manufactured Ti6Al4V is given in [43,60] and this demonstrates a wide range of values obtained in various different studies. In the case of L-PBF tensile samples that were machined from solid bars produced with an ISO certified process for 3D printing of medical devices, the properties obtained adheres to the minimum requirements very well: annealed L-PBF Ti6Al4V with elongation up to 20% was demonstrated [60]. In this case porosity was extremely small (<0.02%), with all pores <0.2 mm in diameter and randomly distributed in the parts. However when complex parts are manufactured, deformations and vibrations of thin features may cause redistribution of powders which can lead to porosity as discussed in [61,62]. The question is – when some larger pores might be present due to various manufacturing errors, at what point does this affect the obtained mechanical properties and become a threat to critical use, e.g. in medical or aerospace applications?

The aim of this overview paper is to present some insight into the effect of defects on laser powder bed fusion materials, especially Ti6Al4V. Prior works have focused heavily on the role of microstructures and also surface roughness [63,64]. In one recent review paper the effects of various manufacturing parameters in L-PBF which affect mechanical properties of parts, including effects of porosity and surface roughness, was examined [65].

The focus of this paper is mainly on porosity and a discussion of various recent studies where the correlation between porosity and mechanical properties is demonstrated. The goal is to improve the general understanding of the role of pores, the criticality of pores, the prediction of mechanical properties and eventual quality control and quality improvement of L-PBF materials. This overview is not exhaustive of the available literature, but rather focuses on the applicability of non-destructive X-ray computed tomography insights and uses some examples from the authors' own work to identify some key trends in this area. In addition, key areas for future work are highlighted.

2. X-ray tomography

X-ray micro computed tomography (microCT or simply X-ray tomography or CT scanning) is an emerging technology used to non-destructively investigate the structural integrity and internal details of samples in various research application fields including materials sciences [26], geosciences [66], concrete and asphalt building materials [67], biological materials [68–71] and also in industrial applications [25,72]. The non-destructive nature of the method allows the investigation of internal defects such as porosity and cracks in parts, in addition to checking geometrical accuracy for all surfaces including complex and internal features. The use of the technique in additive manufacturing is already well-known and various different applications exist as there is a huge synergy between the complexity in L-PBF and the ability to analyze these complex features by X-ray tomography, as discussed in the comprehensive review paper on this topic [29]. Most importantly, the use of the technique to improve process parameters using high resolution analysis of coupon samples holds great promise, as this can help to refine parameters to minimize unwanted defects in the manufacturing process. A schematic of the X-ray tomography process is given in Fig. 1, using the example of a 3D printed sample with internal lattice. The X-ray tomography result shows the presence of powder within the sample between the lattice struts.

It is already widely appreciated that X-ray tomography can be used to detect and measure defects in additively manufactured metals, as discussed above. It is also known as an accurate dimensional measurement device [73]. What is not yet widely known is that when the samples are small enough, the resulting images can be indicative of the type of defect and its cause, as different defects have different characteristic sizes, shapes and 3D distributions. A recent round robin study where parts were produced at various metal L-PBF production facilities and subsequently analyzed by X-ray tomography under identical conditions, showed the presence of a variety of different defect types and distributions, even while all parts had a density over 99.87% [37]. Examples of these are shown in Fig. 2. This analysis was performed using a newly developed standardized workflow for X-ray tomography scanning and image analysis steps, using a 10 mm cube sample of Ti6Al4V [74]. Similar procedures were developed for X-ray tomography-based determination of mean density [75], surface roughness [64] and for powder analysis [76].

The different porosity distributions as seen above arise from different process imperfections. In the examples shown, the irregular random porosity in the first example (sample A) is most likely due to lack of fusion, the cause of which may be non-optimal process-parameters, problems with powder delivering and so on. It seems that this sample was manufactured without contouring and the very rough top and side surfaces indicate the presence of balling effect, which confirms the assumption of non-optimal process-parameters [47]. The porosity in the second example (sample B) is likely due to either an incorrect overlap spacing between contour and hatch scan patterns, or due to keyhole generation at the edges of scan tracks, when the laser slows down to turn around, resulting in higher energy input near the contours [77–80]. Similar

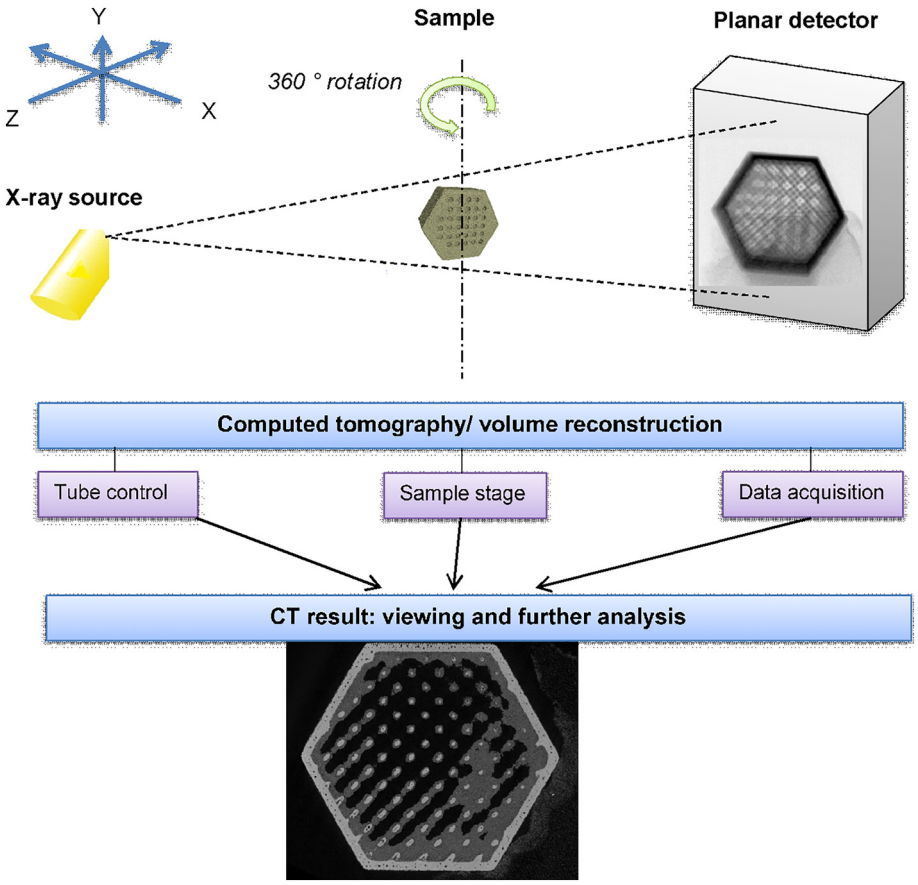

Fig. 1. Schematic of the X-ray micro computed tomography process, taken from [29].

results of keyhole mode pores near the end of scan tracks were shown in [81] with electron beam PBF (E-PBF) of Ti6Al4V components. The third example (sample C) shown contains spherical pores under the top surface of the sample mainly, which is suspected to be keyhole mode porosity that was generated with up-skin scanning of top layers. Clearly these examples illustrate a useful insight into process conditions and provide a tool to optimize these conditions to minimize the porosity distributions in the first place. The transfer of these porosity distributions to complex parts has been demonstrated, but in complex parts additional porosity causes may be present which must also be considered.

3. Effect of defect in castings

In order to build an understanding of the effects of defects on mechanical properties, it is useful to consider cast metals. It is already well known that casting porosity results in poor mechanical properties. The casting process results in trapped gas which creates quite large pores in places – often several mm in diameter. There are methods to minimize the size and extent of this porosity, in particular using casting simulation methods to optimize the injection velocity, the location and shape of casting ingates, and cooling areas on the mold. X-ray tomography is a proven technique to inspect the extent and size of these defects and quality control criteria can be applied. In terms of the effect of these defects, studies have shown that increased porosity in cast metals results in lower tensile strength and lower ductility [82].

Du Plessis et al. [83] manufactured a series of Ti6Al4V investment cast rods, machined to tensile dogbone geometry, with pores all located in the middle of the tensile axis. In a series of tests using X-ray tomography and mechanical testing, it was found by static tensile tests that the failure almost always occurs at the largest pore (despite different microstructures in different batches of samples) and the pore size was inversely correlated with yield strength and ductility. However, even for pores up to 4 mm in diameter in a 6 mm gauge diameter, the yield strength was still close to that of the wrought standard. One sample from this study is shown before and after tensile failure in Fig. 3a. The scan before testing shows the pores with colour coding according to volume, and scanning after tensile test shows the location of failure at the largest pore. In this study, the X-ray tomography data including actual pore geometries were also used in load simulations (finite element analysis) to identify stress concentrations and correlate stress hotspots to failure locations (Fig. 3b).

This approach to apply image-based simulation is increasingly used, since the voxel-based linear elastic simulation is now available without additional meshing steps as was required previously [84,85]. This image-based simulation approach also can be introduced for simulation of AM multi-material parts for multi-scale finite-element simulations to predict mechanical response due to external loading, this has already been done for some civil engineering materials as described in [67,86,87]. The general use of X-ray tomography images for simulations is useful for understanding the effect of defects or inclusions on complex sample geometries.

4. Effect of defect: artificial pores in L-PBF

The previous section demonstrated that relatively large pores found in castings have a definitive effect on the failure location and the resulting mechanical properties of the parts. The general consensus is that casting porosity causes a reduction in yield strength and reduced elongation to failure with increasing pore size. This general rule might be true for additive manufacturing porosity also, but L-PBF pores are typically much smaller and have a different distribution and shape. Utilizing the complexity possible by L-PBF, some work is aimed at creating

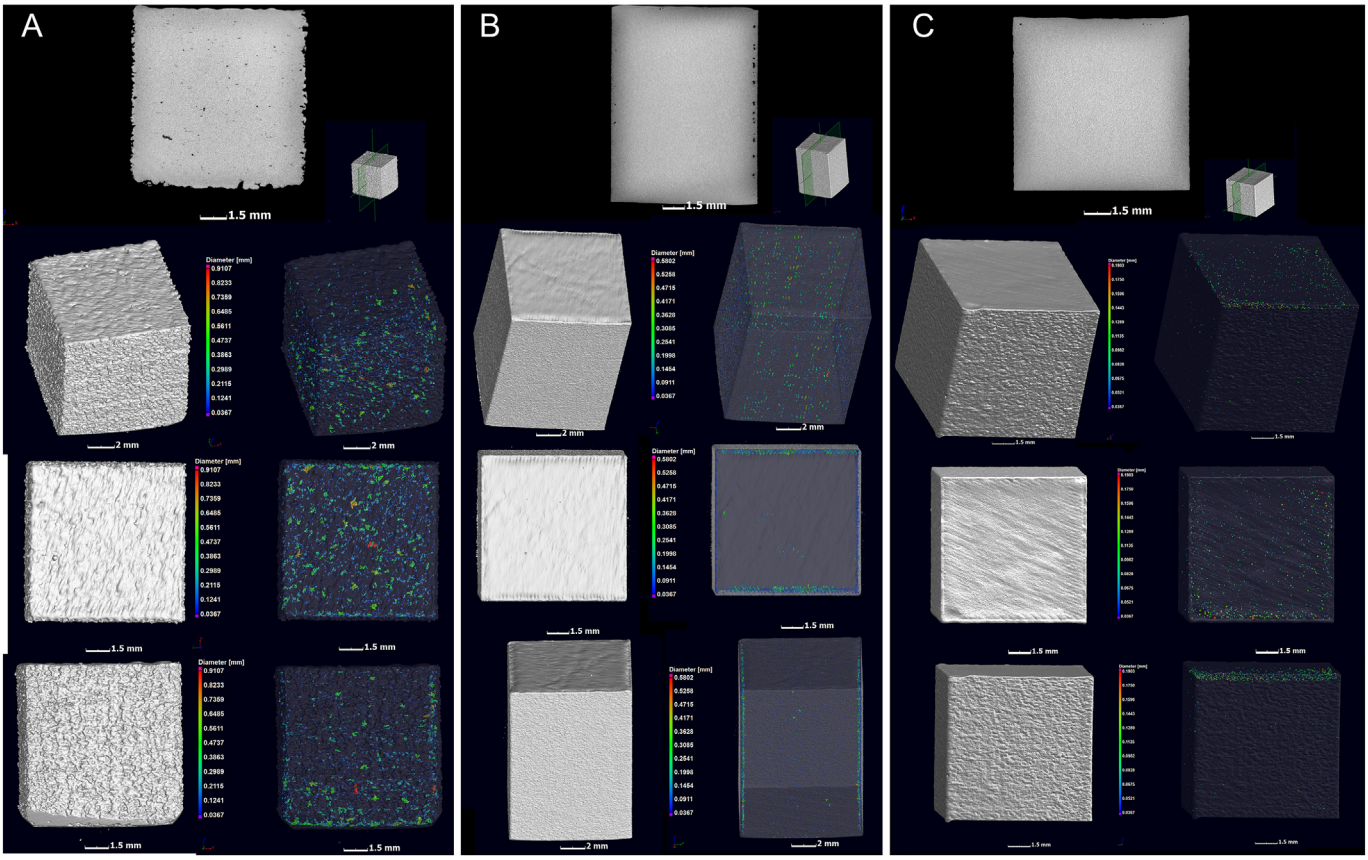

Fig. 2. Examples of different porosity distributions in 10 mm coupon samples. In the three examples shown – each cube (A, B and C) is viewed in CT slice image (top), 3D angled view, 3D from top, and 3D from side. Top is defined in terms of vertical in build direction, so top view shows the top surface of the built cube.
Data taken from reference [37], with new visualizations performed.

artificial pores or defects in parts and then doing mechanical tests to reveal the effect of defect for specific defect types found in L-PBF, this is an active area of investigation, see for example [88]. In experimental data for L-PBF of 316L stainless steel [89], the authors created artificial flat, circular pores emulating lack of fusion, of varying diameters. They showed how the ultimate tensile strength reduced for pores >2.4 mm and elongation was reduced for pores >1.2 mm, in 6 mm diameter tensile rods. Such studies assist in understanding the effect of defect, and many different artificial pore types and locations can be produced for this purpose. In Fig. 4 is shown a test part produced in Ti6Al4V with flaws induced by designing cavities of different thickness from 30 to 180 μm – these X-ray tomography scans were reported in [35,90].

Instead of the designed rectangular shape, the artificial flaw had a complex shape as seen in Fig. 4. The designed and real L-PBF parts differ due to the next layer which was melted and partially closed the gap. The use of artificially designed flaws for test parts is useful for relating mechanical properties to specific pore types and sizes. It is similarly possible to change process parameters to induce specifically lack of fusion pores, keyhole pores or specific defect distributions, by characterizing the process using coupon samples and using X-ray tomography scans. Some examples of coupon samples analyzed from a variety of systems was reported recently in a round robin study [37] and which shows small porosity (the highest value in the series tested was only 0.13%), but specific defect distributions including contour regions, subsurface/upskin pores just under top surface and more. In recent work [91] it was also shown that this region between contour and core part of the L-PBF object is an area that accumulates pores. It would be useful to create mechanical test specimens with each of these conditions and subject these to mechanical tests to determine which are problematic. This is clearly an exciting area for future work.

5. Influence of L-PBF porosity on tensile properties

With optimized process-parameters and scanning strategy, L-PBF porosity is typically quite small in pore size and total volumetric extent and hence it can be expected that the effect on mechanical properties is small. It was found in [92] that values of up to 1% porosity had little effect on the tensile strength or elongation to failure when these defects were caused by excessive energy input (keyhole mode pores, which are rounded). When samples were manufactured at non-optimal process parameters with insufficient energy input (i.e. with lack of fusion defects, typically larger in size and irregular shaped), 1% porosity had a strong detrimental effect on the mechanical properties. As it was shown in [46] generally, variation of elongation values of as-built Ti6Al4V samples is quite wide – 2% up to 9%. The elongation depends on process-parameters, chemical composition of powder and the powder morphology which is a critical influencing factor on the homogeneity of the delivered powder layer. Since L-PBF process is very sensitive to laser power density and temperature gradients, the variation of laser power and spot size for different used systems can lead to large differences in molten pool size and temperature, residual stress and, as a result, high deviations in mechanical properties of as-built samples. A more recent study where Ti6Al4V produced by L-PBF was analyzed by X-ray tomography prior to tensile testing, showed extremely low ductility of as-built samples - <2% - and varied tensile strength values among 6 samples tested in the range 740 MPa to 1220 MPa [93]. This work showed clearly lack of fusion pores in tracks following the laser path, due to lack of fusion between adjacent tracks, as also demonstrated previously in [35]. In other recent work it was shown how the first 100 mm of the build height in a L-PBF system is prone to more lack of fusion pores, resulting in poor tensile properties [94]. Another recent study

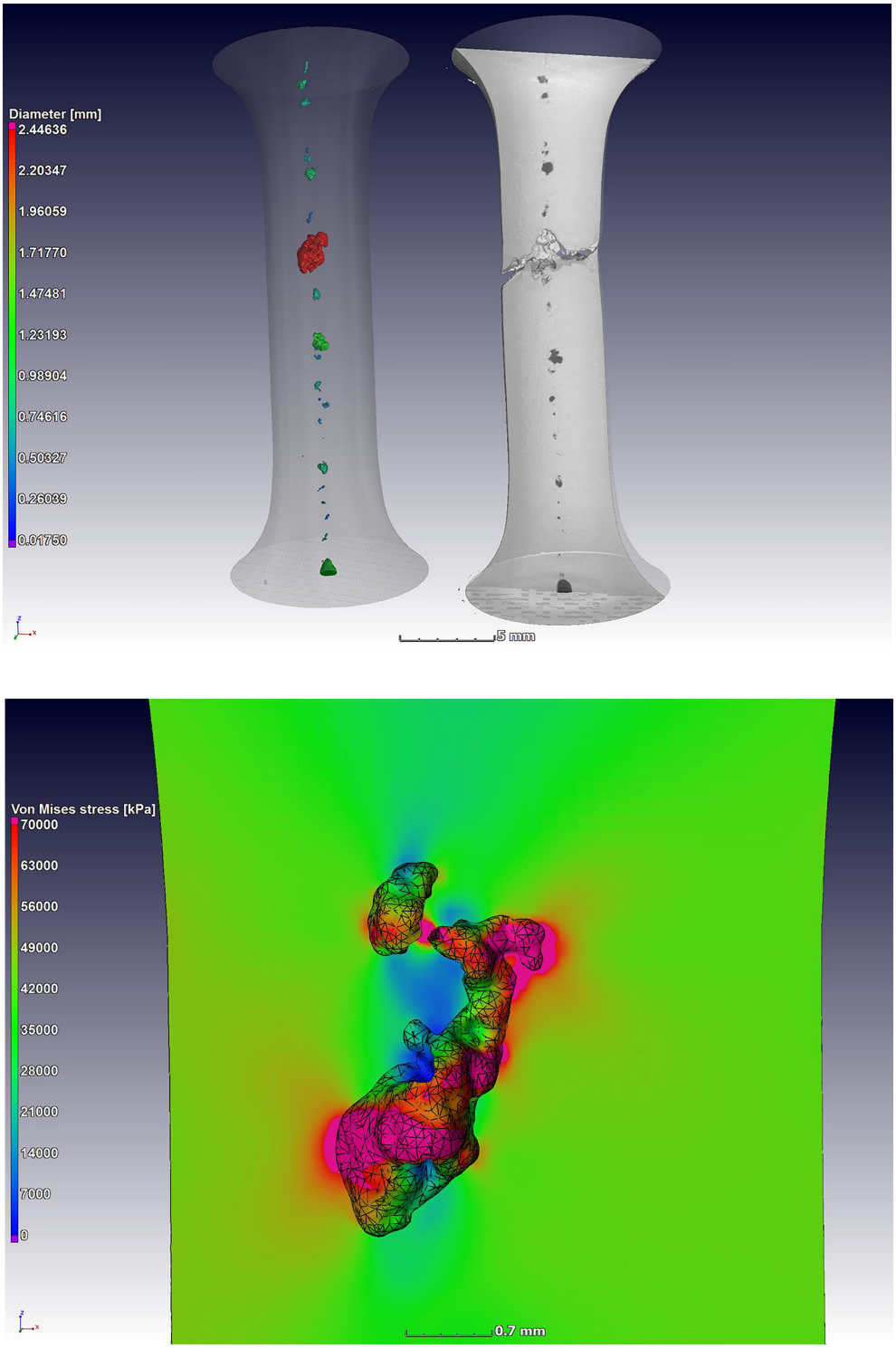

Fig. 3. The effect of defect becomes very clear when imaging casting samples before and after tensile tests using X-ray tomography – failure occurred at the largest pore and simulations including the defect highlight locations of high stress where failure is expected to occur [83].

correlated the presence of porosity to elongation to failure, despite low porosity values for Ti6Al4V produced by L-PBF [95]. A recent study investigated the effect of defects on the mechanical properties of Inconel 625 produced by L-PBF [96]. In this work the authors used X-ray tomography and artificially induced porosity extents in the range of 0.7–1.2% by varying process parameters. It was found that the ductility is strongly influenced by the porosity level but not the ultimate tensile strength.

The use of in-situ X-ray tomography during mechanical loading can be useful to understand the failure process, and for linking the failure to specific defects. In such a study making use of in-situ X-ray tomography during mechanical loading, steel L-PBF samples produced with lack of fusion porosity in low and high quantities (from <0.1% up to 2.2%) were used [97]. It was shown that the higher porosity samples failed at the lack of fusion pores and despite some improvement by annealing, the large-porosity samples still showed poor mechanical properties. This highlights the importance of lack of fusion porosity especially.

In a study of optimized L-PBF of Ti6Al4V ELI [46], X-ray tomography could demonstrate necking extent and analyze the pores in the necking

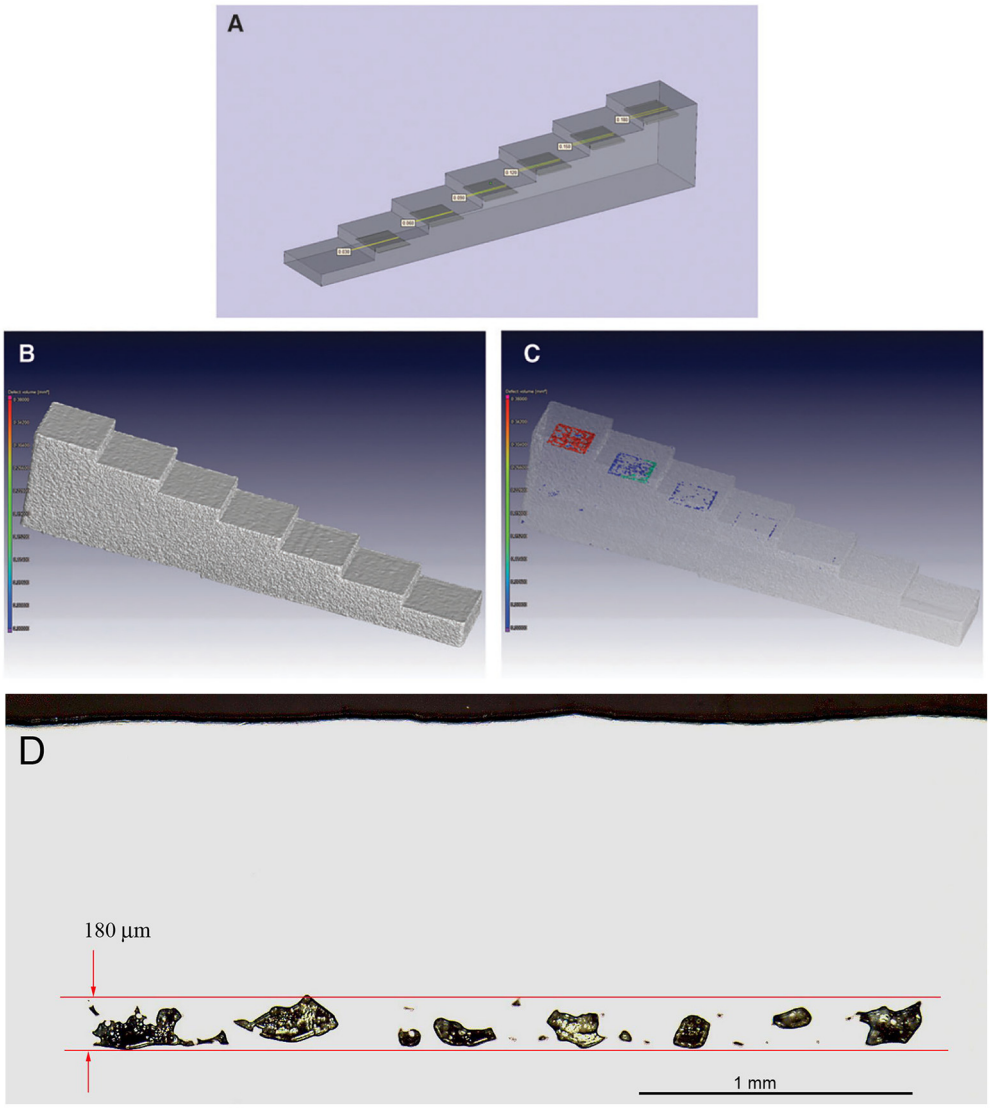

Fig. 4. An example of designed artificial pores and their actual size quantified: designed sample with rectangular flaws (A), CT scan reconstruction of manufactured sample (B, C) and optical microscope image of polished cross-section of designed biggest flaw of 180 µm, from [35,90] (D).

region in pre-strained samples, where pore coalescence occurred prior to complex ductile-brittle fracture in this case (Fig. 5). In this work with samples of porosity 0.002%, the as-built samples machined from solid L-PBF blocks, reached 1265 MPa ultimate tensile stress (UTS) and fracture strain 9.4%. Very low porosity resulted in high strength and elongation with coefficient of variation (a ratio of average value to standard deviation) of 4–6% for as-built Ti6Al4V ELI. With a stress-relief cycle for removal of residual stress and for improving the microstructure, the UTS slightly reduced to 1170 MPa and ductility increased to 10.9%. In a similar study for material qualification for the same process with <0.01% porosity [60], it was shown how annealing can increase the material ductility up to 20%, with a reduction in ultimate tensile strength to 900 MPa. These changes in tensile properties were the result of heat treatments and corresponding changes in microstructure and formation of microstructure close to conventional material.

Anisotropy of mechanical properties for parts built by L-PBF along different angles relative to the build direction (e.g. vertical vs horizontal) is well known and often related to microstructure [43]. In a study by [98], the tensile strengths of the horizontal samples were found to be slightly higher than that of forged specimens, but lower fracture toughness in comparison with forged material was found. It was shown that lack of fusion porosity led to inhomogeneous microstructures and lower resistance to failure of L-PBF specimens. The conclusion was made that lack of fusion defects could be one of the major reasons for the low ductility of manufactured Inconel 718 samples. This conclusion is coherent with results found in [40].

In recent work, it was shown using X-ray tomography and tensile tests, that EBM-produced Ti6Al4V from different build heights have different porosity values and this results in correspondingly different ductility and tensile strength values [99]. The porosity was specifically identified as lack of fusion porosity and its influence on mechanical properties was found to be strongly influencing the ductility (by 20%) and slightly influencing the strength (by 3%), in the range of porosity from 0.08 to 0.003% and maximum pore sizes from 0.2 mm to 0.4 mm.

6. Fatigue properties

Especially for high-end applications such as in aerospace and medical applications, the fatigue properties of L-PBF materials are important. It has been highlighted in numerous works that the pores nearest the surface are most important for fatigue life, while surface roughness, inclusions and microstructure also play important roles [60,65,100–103]. In a study by Brandão et al. [104], AlSi10Mg produced by L-PBF was analyzed using X-ray tomography and fatigue tests. The variation of

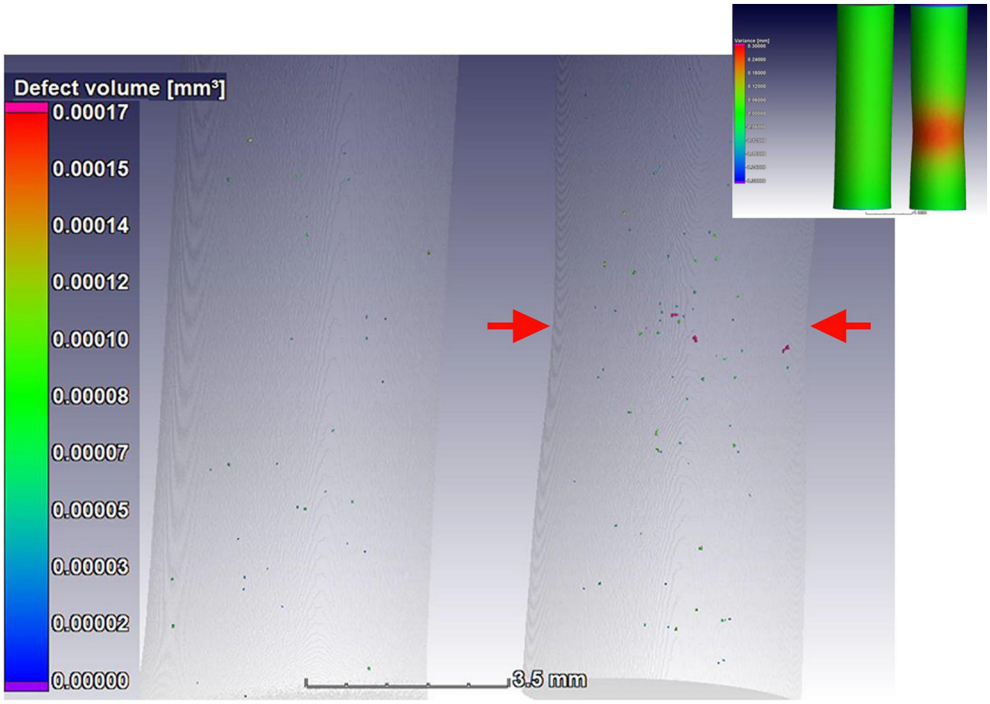

Fig. 5. Time lapse X-ray tomography showing necking creation in stress-relieved Ti6Al4V ELI sample pre-strained from 3.55% to 9.44% from initial length [60].

process parameters resulted in the formation of sets of samples with lack of fusion pores at levels of 0.4–0.8%, and some sets of samples with very low porosity <0.05%. Furthermore, some samples were machined and tested in the as-built state. It was found that the surface roughness of the as-built state results in poor fatigue properties irrespective of the defect populations, indicating the important role of surface roughness for fatigue. Despite this, machined samples with smooth surface also showed poor fatigue properties for those samples with large lack of fusion pores. Best results were found for the combination of machined and low porosity samples. In addition, it was shown that porosity caused by non-optimal contour scanning is detrimental to the fatigue properties.

A literature review on fatigue performance of AlSi10Mg alloy parts produced by L-PBF was recently done by Tang and Pistorius [105]. On the basis of SEM analysis of cross-sections it was shown that different hatch distance and building direction result in different shapes and size of pores that affected the fatigue performance of L-PBF AlSi10Mg parts. Larrosa et al. [106] used Correlative Computed Tomography to estimate the role of defects on the fatigue behaviour of L-PBF AlSi10Mg. It was found that crack-like, or so-called "pancake"-shaped pores act as fatigue crack initiation and propagation sites: if these flat pores are perpendicular to the loading direction, they create high stress concentrations from which fatigue cracks can propagate.

Zhao et al. [107] found that fatigue cracks were initiated from surface or subsurface round gas pores and fatigue life of L-PBF specimens depends on the building direction. Fatigue life was predicted on the basis of average pore size and it was shown that fatigue life decreased with an increase in pore size. Romano et al. [108] studied the HCF and LCF properties of AlSi10Mg produced by L-PBF in the context of prediction of fatigue properties from CT data. They found with statistical analysis, that it is possible to predict the fatigue limit of the material using CT data of witness specimens, which gives a prediction for the fatigue limit of the complex part.

Liu et al. [109] indicated that lack of fusion defects were primarily responsible for fatigue crack initiation in L-PBF Ti6Al4V samples. Location, size and shape of these defects correlated with fatigue life. In another recent study of high-cycle fatigue of optimized L-PBF Ti6Al4V (and annealing heat treatment), it was demonstrated that despite porosity levels as low as 0.02%, almost all high cycle fatigue cracks initiated on pores just under the surface of machined L-PBF samples [110]. A microCT result from this work is shown in Fig. 6, where the fracture surface was analyzed and the "killer pore" identified in fracture surface and in the micro-CT data recorded prior to fatigue testing – the "killer pore" is thus identified and can be compared to other pores in the vicinity. The pore identified as the killer pore in Fig. 6 is near the surface and larger than other pores in the 2 mm region near the identified failure location.

In a similar process, samples were scanned before and after 3-point bend fatigue tests, for L-PBF of aluminium alloy, containing subsurface porosity. The crack can be visualized and its location and growth can be followed in X-ray tomography images, as shown in Fig. 7. In this example, the crack passes through a pore near the surface, which has a diameter of ~0.2 mm.

A recent example of the importance of near-surface pores as critical crack initiation pores is given in [111], where samples were produced with high density contours and very porous interiors using process parameters leading to lack of fusion pores. Crack initiation occurred on pores within 0.1 mm of the surface, despite much larger and higher values of porosity on the interior of the samples, in high cycle fatigue tests. The use of X-ray tomography clearly identifies pore distributions and helps to correlate killer pores on the fracture surface with those in X-ray tomography data. Analysis of CT scans and SEM micrographs of fracture surfaces in the fatigued specimens that was done in [112] showed that pores which occurred near the surface (in the outermost 400 μm thick layer) promoted crack initiation. In HIPped samples, at long fatigue life, crack initiation occurred near very small pores (20 μm), while at short fatigue life, the crack nucleated just from a shallow crater.

Another study [113] of the static and fatigue properties of L-PBF steel, without using X-ray tomography, revealed a few interesting observations with regards to lack of fusion defects and their effect on mechanical properties. Static tensile properties were found to be superior to that of the wrought standards in all respects, despite the presence of large lack of fusion defects. Fatigue properties of different build orientations and high and low cycle regimes were conducted, with as-built surfaces and with polished surfaces. It was found that good fatigue properties are found for all conditions, while high cycle fatigue

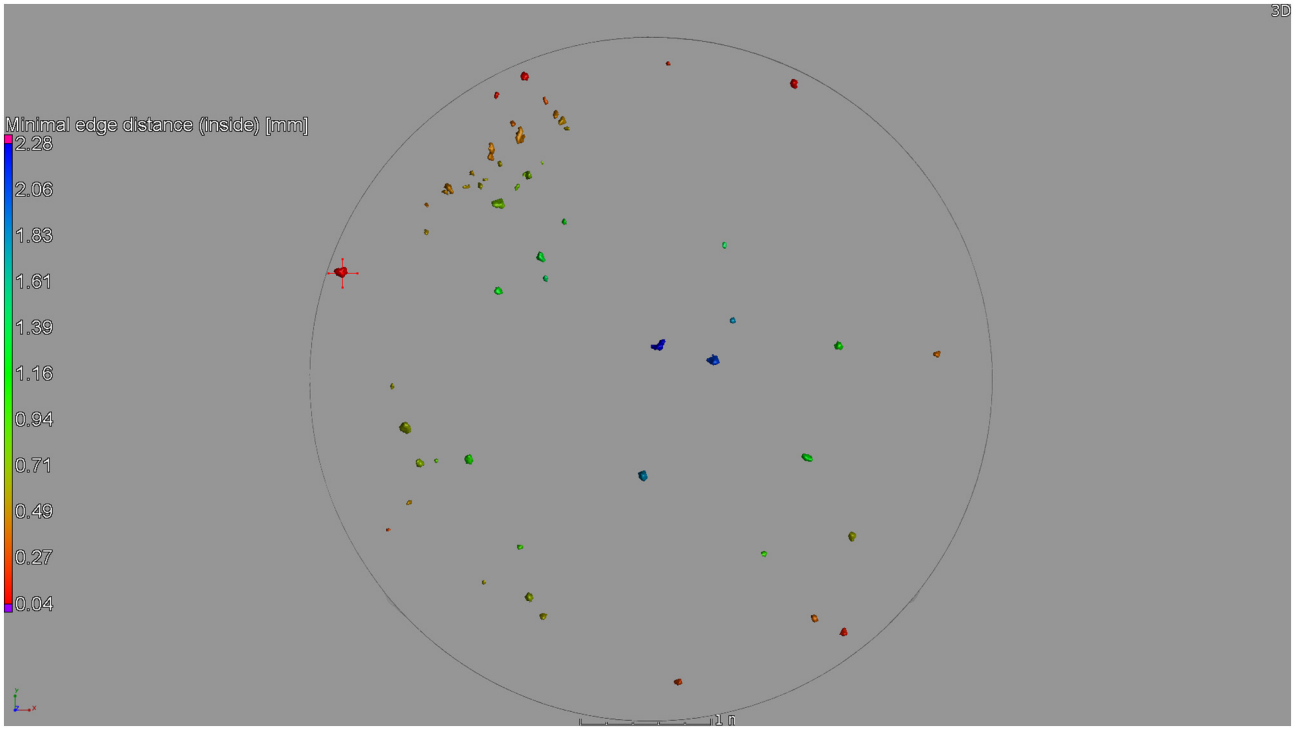

Fig. 6. Fracture surface analysis and X-ray tomography prior to fatigue tests, allowing visualization of all pores in region of failure – highlighting the "killer pore".

variations could be attributed to the orientation of the planar lack of fusion pores relative to the loading direction. Failure also occurred primarily on near-surface pores.

In electron beam melting (EBM) samples with porosity, high resolution X-ray tomography was used to attempt a ranking of pore likelihood to act as crack initiator in fatigue tests [114] with some success, when using surface proximity and pore aspect ratio. This again highlighted the capability to use tomography to provide a clear identification of the role of defects.

7. Post processing

Hot isostatic pressing (HIP) is already a widely used process for closing pores and improving the microstructure in metal parts in general [115], and for additively manufactured metals in particular [48,116]. In a study of cast Ti6Al4V, relatively large pores in the centre of rods were imaged by X-ray tomography before and after HIP processing, one example is shown in Fig. 8, where almost all pores are closed to below the resolution limit of the instrument

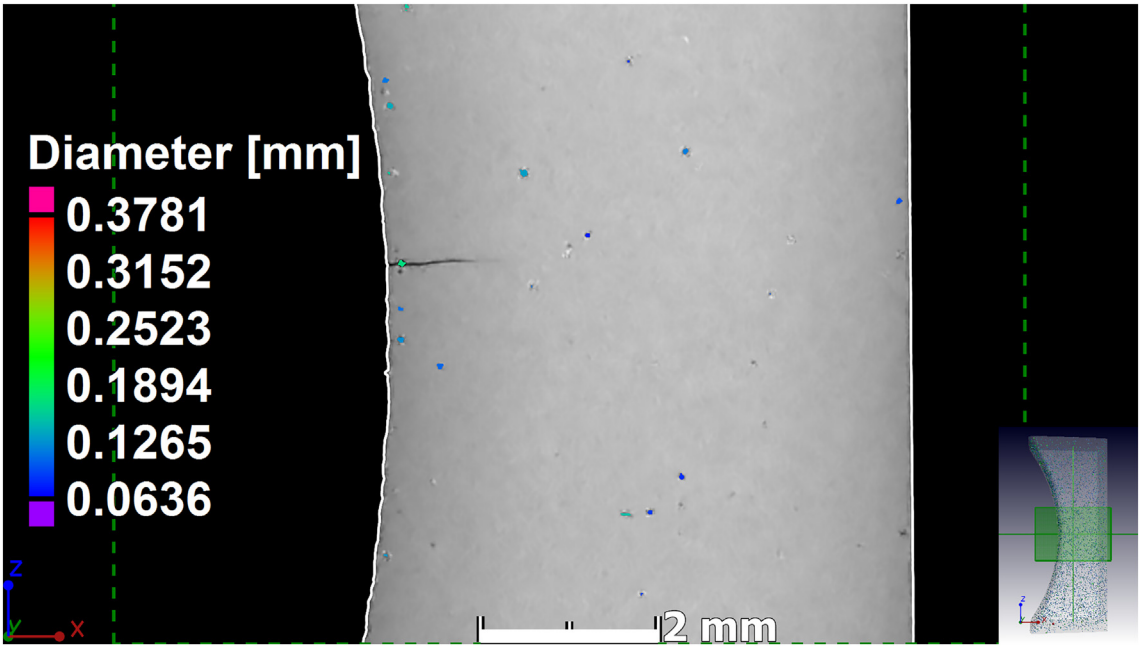

Fig. 7. Example of 3-point bend test sample of L-PBF AlSi10Mg, with as built surface roughness and porosity near surface – in this case the crack has formed >1 mm and passes through one of the largest pores near the surface (green). (For interpretation of the references to colour in this figure legend, the reader is referred to the web version of this article.)

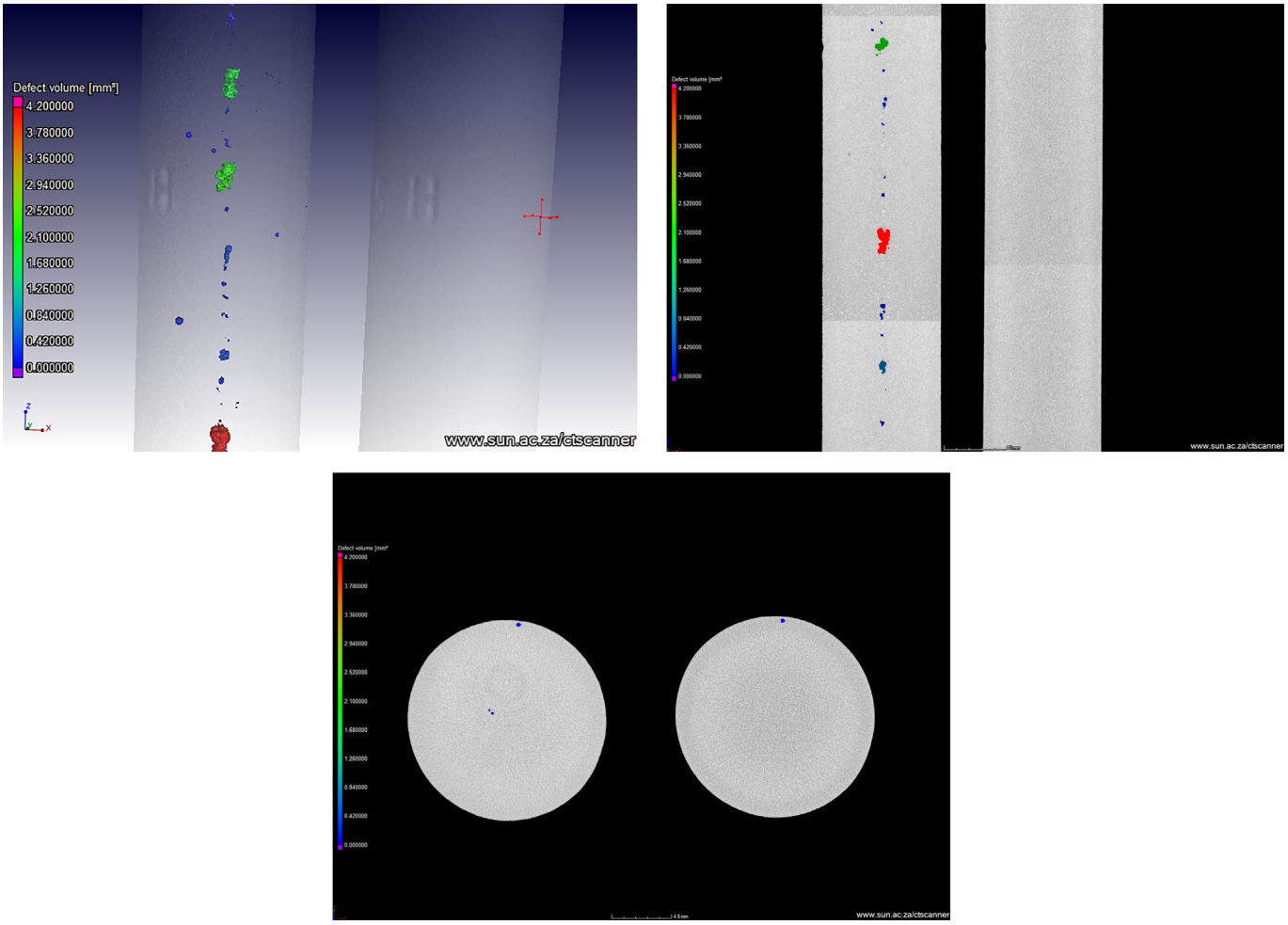

Fig. 8. X-ray tomography of cast rods before and after HIP processing showing effective closing of pores. The example shows large pores closed very effectively (as seen in 3D image), but some near surface pores are not affected - for example shown in the slice image.

(from 4 mm down to <0.02 mm), except some selected pores near the surface. This is likely due to the presence of an alpha case layer at the surface which is prone to microcracks, invisible to the X-ray tomography images, but allowing penetration of Argon during the HIP process, making the process ineffective for these pores.

While the HIP process is very effective, alternative processes might be valuable. The effect of different surface processing techniques on fatigue properties was already mentioned in the section on fatigue properties, especially in the study [104] the rough surface was highlighted as more important for fatigue properties than the internal defect population. This study also found, with the given process parameter set, that contour scanning created subsurface pores which were detrimental to the fatigue properties, and scanning without any contour track improved the fatigue properties more than any jet blasting or vibratory finishing surface processing of the as-built surface.

Considering the importance of subsurface pores and the surface roughness of as-built specimens, surface enhancement processes are highly important. Popular methods include shot peening [117,118] and laser shock peening [119], both of which have been shown to improve mechanical properties. This improvement is widely attributed to the compressive stresses induced at the surface and the improved surface finish, but recent work shows also that near-surface pores were closed by laser shock peening of L-PBF AlSi10Mg, as shown in Fig. 9 [120].

8. Process parameters

As mentioned in the section on X-ray tomography, different porosity types are present in L-PBF and can be distinguished by X-ray tomography – typically these are categorized into lack of fusion, metallurgical pores and keyhole mode pores. Various other distributions may exist due to the complex interrelationship of the laser scan strategy, hatch distance, layer thickness, laser power and scan speed, etc. In situations where the energy density is high (slow speed and high power), the high energy creates an unstable vapour depression which closes in on itself during movement of the meltpool, creating keyhole pores [32,121]. At too low power or fast scan speed, there may be lack of fusion between adjacent tracks or between successive layers on top of each other, due to the track width and depth being too small. The overlap of successive tracks and layers can result in remelting which can reduce porosity or modify existing pore distributions. Slowing at the end of scan tracks, or incorrect hatch and contour spacing/offset can create pores near the surface of the part. All of this is demonstrated beautifully in recent synchrotron X-ray imaging efforts helping to improve the understanding of different pore formation mechanisms in laser powder bed fusion [77,121–123]. The processes are also described in [124] and Fig. 10 is taken from this work, indicating the porosity variation in L-PBF cube samples produced at varying laser power, all other parameters kept constant. This shows the regimes of lack of fusion, optimized parameters with porosity ~0.01% and increasing amounts of keyhole mode porosity up to almost 0.5% as laser power is increased. This

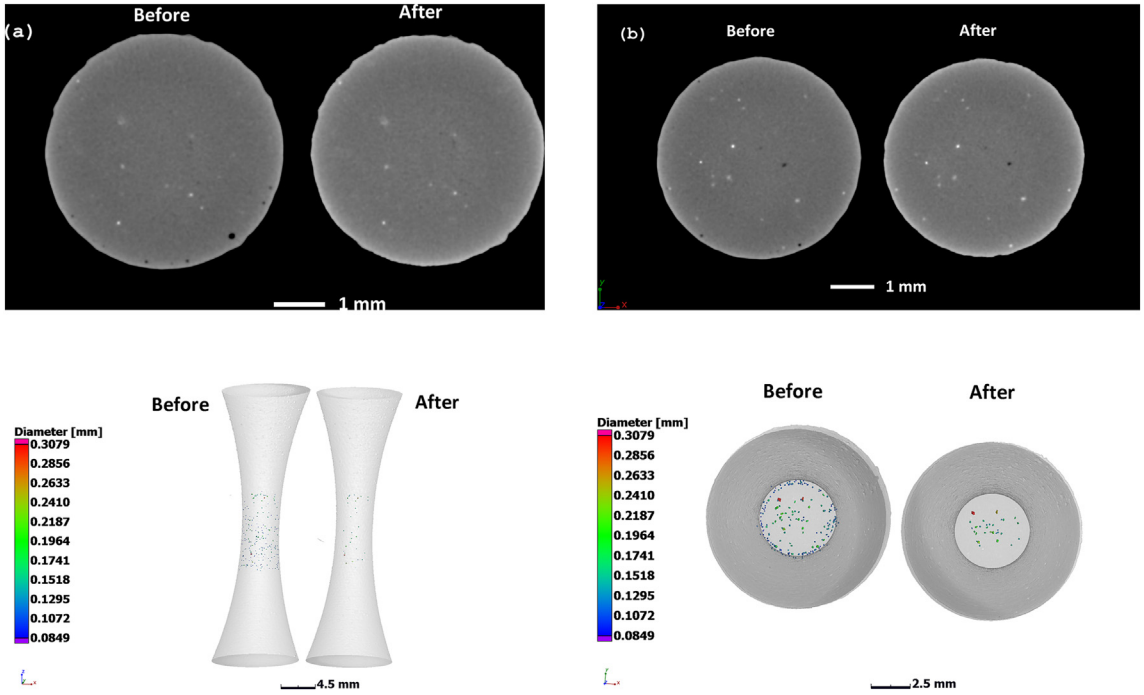

Fig. 9. Laser shock peening closes near-surface pores in L-PBF-produced AlSi10Mg as demonstrated by X-ray tomography before and after processing in slice images and 3D views from front and top.
From [120].

work demonstrates the changes in size and morphology of typical defects found in L-PBF processes. Another recent study elaborated on typical defect morphologies present in two different L-PBF systems for a thin-walled test sample, where the pore morphology and sphericity was studied as a function of location and repeatability in different systems used [125].

It is important to realize that despite optimized process parameters, variations during processing can create areas with increased porosity. For example, as shown in Fig. 11, the down-skin areas at the underside of a complex part where the supports were connected, is typically prone to increased porosity. This might be due to irregularity on the powder bed at these locations due to the solid supports with powder in between, causing uneven powder spreading, or it could be due to thermal differences – in unsupported areas between supports, there is less thermal conduction raising the local temperature which can increase the likelihood for keyhole mode porosity. While these are speculative ideas and requires further study, it is clear that the process itself may cause porosity which is not regularly spaced especially in complex shaped parts, and optimizing process parameters is therefore not enough, inspection of final parts is also necessary.

9. Complex-geometry parts

Evaluating the effect of defects on standard test geometries is important, but how does this relate to complex geometries as realized by laser powder bed fusion? For example it is possible with L-PBF to realize parts

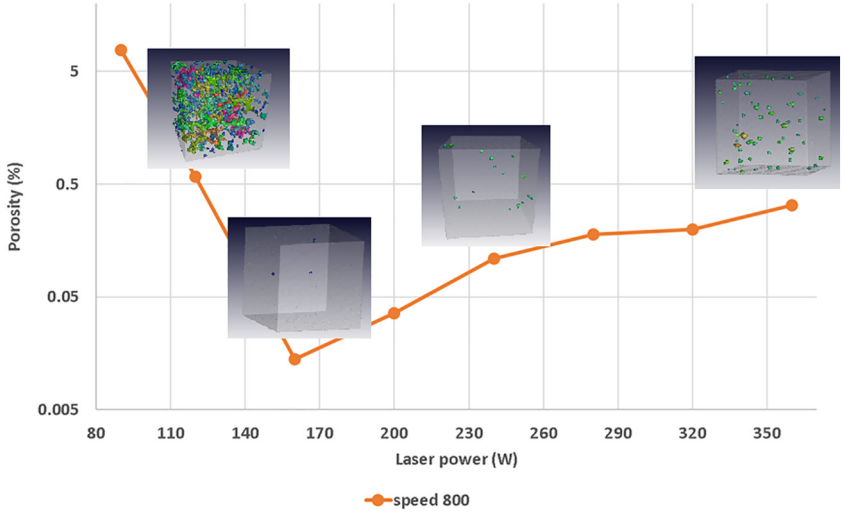

Fig. 10. Porosity variation with laser power and 0.8 m/s scanning speed for L-PBF Ti6Al4V using an EOS M290 system – all other process parameters according to their default values for 30 μm powder layer thickness. Note the log scale on the y-axis.
Image from [124].

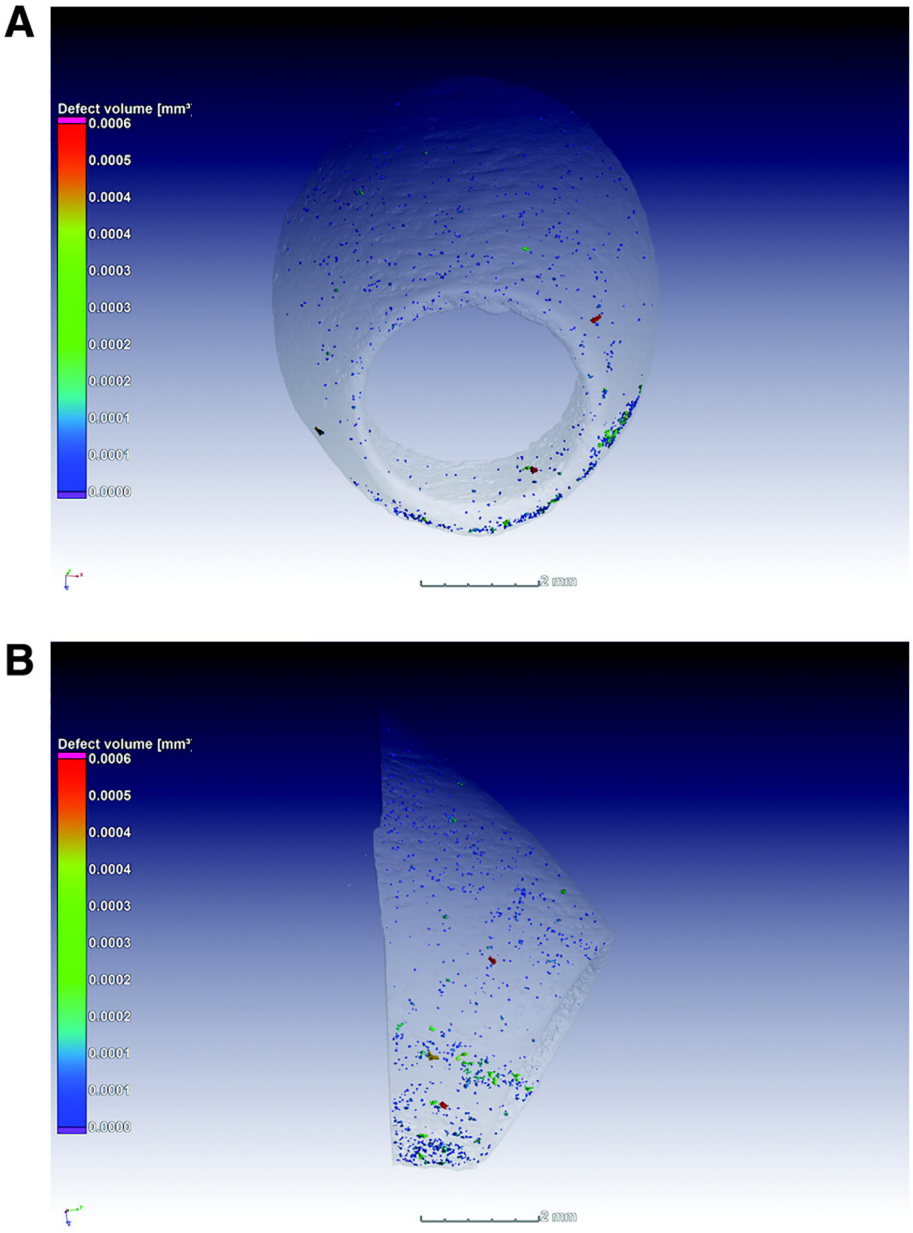

Fig. 11. An example of increasing porosity on down-skin areas, taken from [126].

with biomimetic designs with organic shapes, cellular or lattice structures or combinations of complex design approaches [7]. Often these parts contain thin walls or struts, and rough surfaces which are not accessible for post processing, and therefore the as-built surface roughness of such inaccessible locations may act as crack initiation sites (as notches effectively). Since the struts or walls are thin in places, having a pore in such a thin section, even if it is very small, may have a strong influence on the mechanical performance of the part. Here X-ray tomography plays a crucial role for checking surface quality and pore locations. Quantifying the surface roughness and porosity using tomography allows to determine quality approval criteria, but destructive tests might still be required to validate this choice, as it cannot easily be predicted what the effect of such defects might be. An example of a cubic lattice produced by L-PBF is shown in Fig. 12, with its CAD design geometry also shown in purple. There are clear deviations from the design, on all surfaces. Such relatively large deviations can be expected to have an influence on the mechanical properties. Also visible in Fig. 12 at the top left is a spherical pore space designed and intentionally produced for investigating its effect on the mechanical properties of the lattice structure.

Sometimes simulations can assist in minimizing the amount of destructive testing – specifically using the same X-ray tomography data and making image-based simulations of the part design compared to its actual geometry and pores. This calculates the effective elastic modulus and Von Mises stress values, highlighting the importance of pores in specific locations: this was demonstrated in [83,127]. A study was performed in [128] where a cubic lattice (very simple lattice with vertical load bearing struts) was designed with a single 0.5 mm diameter intentional pore in a single load bearing strut of 0.8 mm diameter (as in Fig. 12 above). X-ray tomography validated the presence of the pores and compression tests were performed on control and defect samples – all produced by L-PBF in Ti6Al4V and stress-relieved prior to testing. The results are shown in Fig. 13. Surprisingly, the yield strength was not affected by the

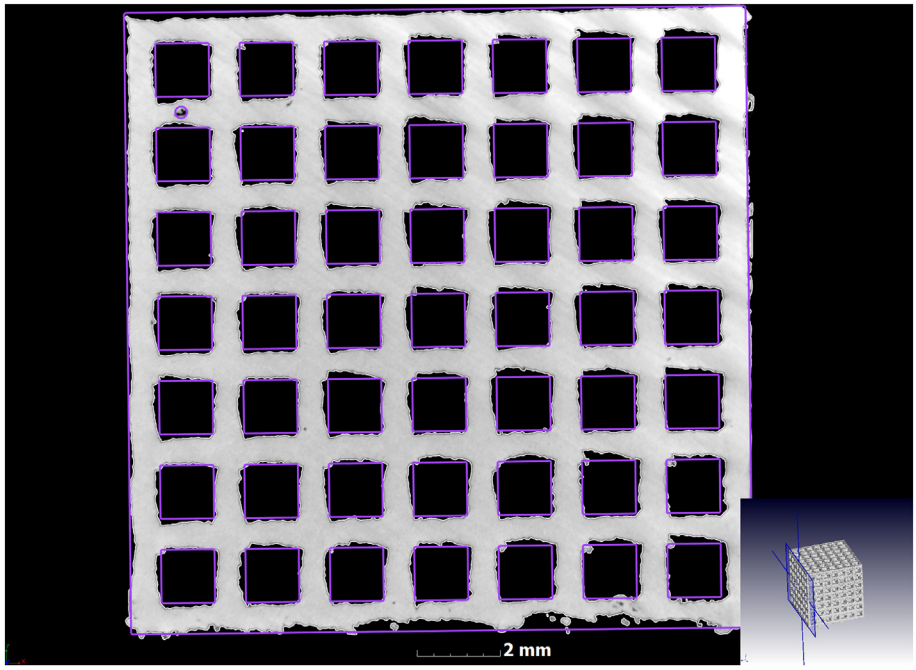

Fig. 12. Comparison of actual L-PBF lattice with its CAD design. An intentional designed pore space is included and is visible in the top left of the structure.

presence of the pore. This could be explained by simulations where it was shown that the actual geometry compared to the ideal geometry shows much larger differences than between samples with and without pores. Effectively it shows that the lattice geometry is more important than the internal defect size. This is for an ideal spherical pore in the middle of a single strut in static compression

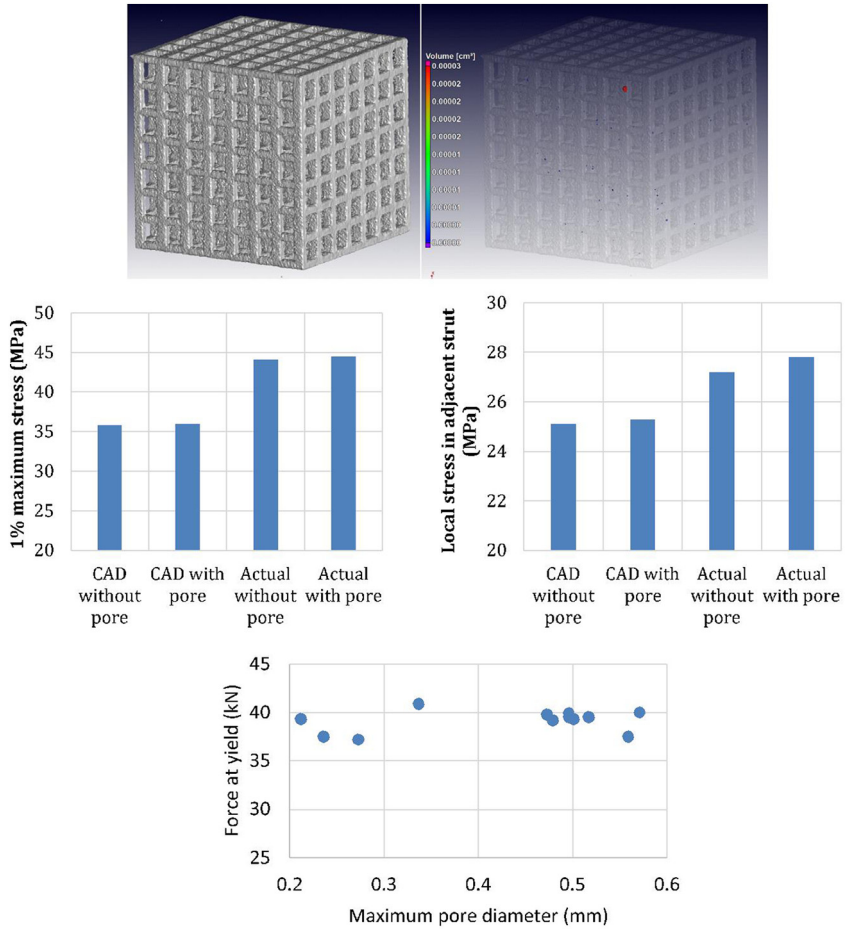

Fig. 13. Effect of defect in a single load bearing lattice strut, on compressive strength.

loading only, but is nevertheless promising. It demonstrates the importance of design, and the fact that not all pores are harmful.

10. The role of simulations and property predictions from CT data

Thermal simulations of the layer by layer build process is increasingly used to assist in design modifications, appropriate placement of support structures and the choice of best orientation of the build in the chamber, to minimize thermal hotspots which leads to residual stress and even cracking of parts during build [129–131]. These simulations might also be useful for predicting areas of porosity, as increased thermal buildup results in effectively a form of pre-heating and hence a higher thermal input into the meltpool – this can result in the formation of keyhole mode pores in some areas and not others, for example, depending on the local thermal conditions during the build. Appropriate build simulation and appropriate design might mitigate this, and it might also be possible to implement in real time power control to modify the meltpool to maintain constant and stable tracks despite local thermal changes, reducing porosity as well as residual stress. These are exciting areas of development for the near future [132].

In another simulation-based approach, traditional finite element analysis can be used to understand the effect of defects on parts. This was done for typical pore sizes and shapes in recent work, for assessing the effect on fatigue strength, based on cross-sectional pore information [133]. This can be done using X-ray tomography data of the actual part including its defect, or on idealized models with artificially induced pore spaces, also in complex parts. In Fig. 14 is shown an ideal model of a cubic lattice with load applied vertically downwards, with pore space in a load bearing strut. The close-up view shows the local high stress at the sides of the pore – quantifying this stress value and the local stress in the adjacent strut, as a function of varying pore size, allows to understand the role of the pore in reaching a critical stress value. In Fig. 14 is shown that in this case the stress next to the pore only becomes larger than the stress in the adjacent strut, for pores larger than 0.1 mm in pore diameter – hence the geometry plays a larger role up to this point. The increase is also not as sudden as might be expected, but this is of course for an ideal spherical pore space, in the middle of the strut.

Expected loads and constraints are applied and simulations show stress hotspots and can even be used to assess effective elastic modulus of the structure – e.g. lattice structures of different designs as in [134]. Similarly, two designs were compared in physical mechanical tests compared to simulations and the simulation stress hotspots corresponded to the initial failure locations and indirectly to the failure modes in layer-by-layer and diagonal failures in [135].

Dallago et al. [136] compared the mechanical properties of predicted as-designed lattice structures and produced L-PBF samples and highlighted that it is strongly influenced by the defects (notches, geometrical deviations from design) and residual stress that was introduced by AM process. It was also noted that the combination of micro X-ray tomography with FE simulations permits to investigate effect of L-PBF defects on the mechanical properties in-depth.

The use of load simulations can be particularly useful in studies where the as-built surface and internal defects are both present, possibly including a complex design – in that the most important factor is not clear and a combination of effects result in the complex stress distribution. Another approach is to use statistical models to estimate the influence of defects on the mechanical behaviour. Romano et al. [108] have investigated the use of statistics of extremes to estimate the critical

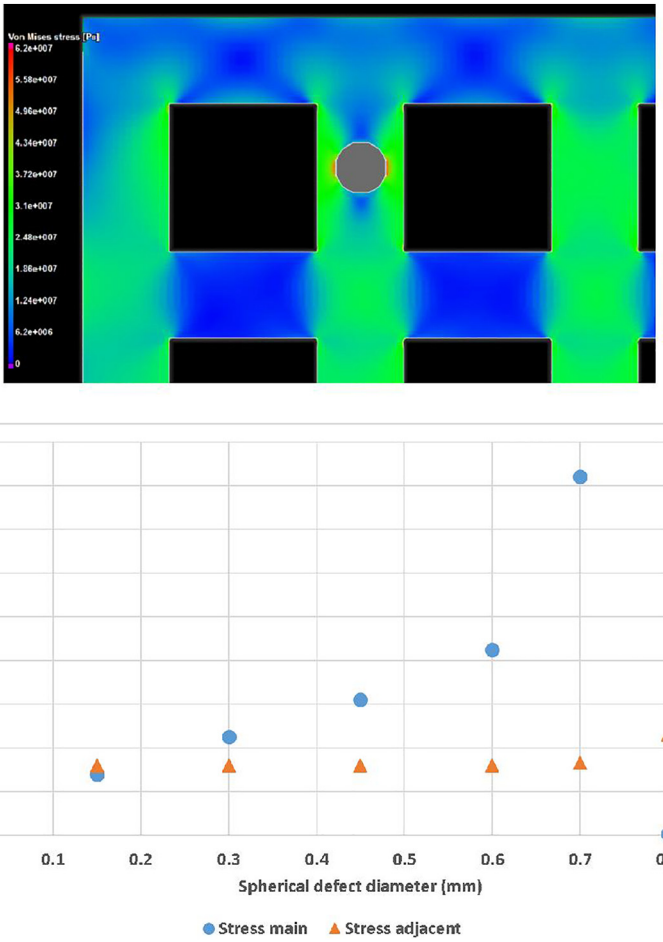

Fig. 14. Finite element analysis simulations can be used to evaluate the effect of defects, as shown here for an ideal lattice design, from [128].

defect size, which may be used as part of a quality control process, for example. Recent work has extended this concept to understand the importance of volumetric defects as compared to surface flaws [137].

11. Implications of critical pore sizes

The understanding that larger pores are more important for mechanical properties, and that very often pores smaller than some critical size – for example 0.5 mm – make no difference to the mechanical properties of a part, is an important general result which builds confidence in the capability of L-PBF. Despite small pores, mechanical properties can be excellent and if pores are kept small, the critical factors affecting the mechanical properties shift towards microstructure, surface roughness and part geometry, irrespective of the material type. When pores become larger than some critical size - for example 0.5 mm - they start to play a significant role and may overtake these others as the critical feature affecting mechanical properties and leading to premature failure. The relative importance of pore size and extent depends on material type and this needs to be further investigated for an even better understanding in future work. For example, the critical pore size in Ti6Al4V might be 0.5 mm while in Inconel it could be 2 mm. It must be kept in mind that this is a major simplification and it is possible that clusters of small pores may act as a single large pore, pores located along a line or plane perpendicular to the load direction may be critical even though the individual pores are very small, or a pore very near a surface may be more critical and hence smaller pores are more important in those special cases. This all requires further study to unravel the relative importance of each effect.

With this kind of information of critical pore size it is possible to address the situation in a number of ways. The first is to minimize process-induced porosity such that pore sizes are below the critical size. This is easily achieved in commercial L-PBF systems as demonstrated widely already. In addition to process parameter optimization, unexpected pores can be formed during the L-PBF process which are not related to process parameters. These unexpected pores can be identified by in-situ monitoring using various techniques currently under development. Post-production testing by X-ray tomography is an obvious solution but is relatively expensive and therefore only used for highly critical applications thus far. The fact that only roughly 0.5 mm pores and larger necessarily need to be detected can greatly simplify the X-ray tomography process and hence reduce scan times and costs. For example, scanning a 20 mm-diameter part at 20 μm voxel size allows accurate quantification of all pores >27 voxels in extent (a cube of 3x3x3 voxels), which relates to pores >60 μm. By scanning at the same quality (voltage and exposure time, etc.) but at voxel size of 100 μm, all pores >0.3 mm will be quantified but the number of projection images is reduced due to the lower magnification. This relates to scan time reduction in this example from 1 h to 10 min, for example. Alternatively, more of the same size parts can fit into the field of view and e.g. 8 parts can be scanned in 1 h. Depending on the part geometry and material type, scanner type and required scan quality, optimized scanning is possible for high throughput of samples in different permutations as explained above.

It should be emphasised here that this critical value of 0.5 mm is a simplification for the case of optimized L-PBF process parameters and not for situations with regularly spaces pores along scan tracks, or similar non-random pore distributions. This simplification also ignores some other factors which can influence the mechanical properties, which cannot be detected by X-ray tomography. For example, oxidation during the L-PBF process due to shielding gas problems causes brittle material properties. Residual stress and microstructure are invisible to X-ray tomography and may be critical in some cases. X-ray tomography also has other limitations and is clearly not a single solution to quality control. For example, very high voltages are required for steel and other metals with high atomic mass compositions, as these absorb X-rays very strongly. Many desktop microCT instruments are not suited to this sample type, even when the samples are very small. Larger X-ray microCT instruments are expensive to maintain and hence less widely available at present. There are also still varied methods for quantification of porosity from 3D images, image quality differences between different X-ray tomography instruments, operators using different scan settings and sometimes inducing image artifacts, all of which can affect the obtained results. Therefore continued work in developing standards and simplified workflows for X-ray tomography is important, as is the fact that it should be used in combination with other quality control tools.

12. Conclusions

This review paper has focused on the effect of defects on the mechanical properties of metal L-PBF parts. It is increasingly becoming clear that L-PBF materials always have small pores present in varying degrees and this porosity might vary in its extent, distribution and morphology depending on the system used, the powder used and the process parameters used, among others. The effects of these pores might be detrimental to the mechanical properties of the produced parts and this is not always well understood or predictable. It has been shown in a range of examples how small pores up to 0.5 mm and total porosity extent up to 1% often seem to make no difference – surface roughness and part geometry are much more important and failure mechanisms are mainly driven by microstructure [138]. While exceptions might occur, for example for layered flaws with large extent, the main message is that in most cases the small porosity present is harmless for strength and ductility in static loading conditions. With increasing porosity the strength is reduced and the ductility is also reduced, and the failures are likely to initiate at the largest pores. In most studies it was shown that ductility is more strongly influenced by the porosity than the strength. It should be emphasised that porosity formation up to levels where this is a problem may occur easily when a L-PBF system has some error, and many things can go wrong which pushes the porosity above this level. These sizes of pores and levels of porosity are easily identified in X-ray tomography and while one of the disadvantages of X-ray tomography is the limited resolution for large objects, the above-mentioned relatively large critical pore size means that only the largest pores are really important, so quality control criteria can be adjusted. This has implications for faster tomography scans and higher throughput. It is also clear that current commercial L-PBF systems easily achieve better than 0.13% porosity as demonstrated in a round robin test [37]. Despite this positive trend, some pore types are problematic. Specifically lack of fusion pores are more irregular and have been shown to be more detrimental to mechanical properties than other forms of porosity, so special care must be taken to ensure no lack of fusion occurs (high enough power, close spacing between tracks and layer thickness is small enough).

Fatigue properties are more critical to total porosity extent and proximity of defects to the surface, with pores within 1 mm of the surface typical crack initiators and the largest such pores will likely be the killer defects. This has been underestimated until now but the use of X-ray tomography and the advances in quality of L-PBF materials has led to the identification of near-surface pores as critical for fatigue applications (and the fact that these often occur in AM materials). One solution to improve density is by process optimization and quality control – this is practically possible and has been demonstrated for Ti6Al4V. Improvements in the reproducibility of CT-based quantification of such small levels of porosity is only now becoming possible by standard workflows for X-ray tomography analysis of coupon samples, so more work in other materials is required for this approach. The other approach is post-processing to remove these pores. One well-known and widely used post-processing method is HIPping. While it works extremely well, it has specifically been shown to be ineffective for pores very near (or open to) the surface in selected cases. Another alternative is the use of shot peening or laser shock peening, which not only induces

compressive stress in the material but also partially or fully closes near-surface pores.

The quality improvement of L-PBF processes and the increased confidence in the use of this process for production is highly important – for primary load bearing structures and mission-critical parts. An improved understanding of which defects are critical and which are less important can help in quality control, quality improvement and for development of better post-processing techniques and other ways to increase reliability and reproducibility of high quality metal L-PBF parts. There will never be a precise rule to determine the threshold for the size or location or some value which exactly defines a pore to be dangerous or not, especially considering the wide range of production processes (different L-PBF scan strategies, powers, etc.) and different materials. Some materials may be more prone to defect-driven failures while others may be driven more strongly by microstructural effects. Despite this, there is an interest to improve our understanding of the effects of defects on mechanical properties in general and specifically for popular L-PBF materials such as Ti6Al4V and AlSi10Mg. Central to understanding defects is the use of X-ray tomography to unravel the true effect of defects non-destructively, and we hope this work stimulates more work along these lines to continue this process and reveal practical "rules" which may be broadly applicable.

CRediT authorship contribution statement

Anton du Plessis: Conceptualization; Writing - original draft; writing - reviewing and editing. **Ina Yadroitsava:** Investigation; writing - review and editing. **Igor Yadroitsev:** Investigation; writing - review and editing.

Declaration of competing interest

The authors state no conflict of interest in this work.

Acknowledgements

The Department of Science and Innovation, Republic of South Africa is acknowledged for support through the Collaborative Program for Additive Manufacturing (CPAM). This work is also based on the research supported by the South African Research Chairs Initiative of the Department of Science and Innovation, Republic of South Africa and National Research Foundation of South Africa (Grant No 97994).

Data availability

Data is available on request.

References

[1] T. Debroy, H.L. Wei, J.S. Zuback, T. Mukherjee, J.W. Elmer, J.O. Milewski, A.M. Beese, A. Wilson-Heid, A. De, W. Zhang, Additive manufacturing of metallic components – process, structure and properties, Prog. Mater. Sci. 92 (2018) 112–224, https://doi.org/10.1016/j.pmatsci.2017.10.001.

[2] D.D. Gu, W. Meiners, K. Wissenbach, R. Poprawe, Laser additive manufacturing of metallic components: materials, processes and mechanisms, Int. Mater. Rev. 57 (2012) 133–164, https://doi.org/10.1179/1743280411Y.0000000014.

[3] D. Herzog, V. Seyda, E. Wycisk, C. Emmelmann, Additive manufacturing of metals, Acta Mater. 117 (2016) 371–392, https://doi.org/10.1016/j.actamat.2016.07.019.

[4] M. Schmidt, M. Merklein, D. Bourell, D. Dimitrov, T. Hausotte, K. Wegener, L. Overmeyer, F. Vollertsen, G.N. Levy, Laser based additive manufacturing in industry and academia, CIRP Ann. 66 (2017) 561–583, https://doi.org/10.1016/J.CIRP.2017.05.011.

[5] C.Y. Yap, C.K. Chua, Z.L. Dong, Z.H. Liu, D.Q. Zhang, L.E. Loh, S.L. Sing, Review of selective laser melting: materials and applications, Appl. Phys. Rev. 2 (2015), 041101. https://doi.org/10.1063/1.4935926.

[6] D. Bourell, J.P. Kruth, M. Leu, G. Levy, D. Rosen, A.M. Beese, A. Clare, Materials for additive manufacturing, CIRP Ann. 66 (2017) 659–681, https://doi.org/10.1016/J.CIRP.2017.05.009.

[7] A. du Plessis, C. Broeckhoven, I. Yadroitsava, I. Yadroitsev, C.H. Hands, R. Kunju, D. Bhate, Beautiful and functional: a review of biomimetic design in additive manufacturing, Addit. Manuf. (2019) https://doi.org/10.1016/J.ADDMA.2019.03.033.

[8] J. Liu, A.T. Gaynor, S. Chen, Z. Kang, K. Suresh, A. Takezawa, L. Li, J. Kato, J. Tang, C.C.L. Wang, L. Cheng, X. Liang, A.C. To, Current and future trends in topology optimization for additive manufacturing, Struct. Multidiscip. Optim. (2018) 1–27, https://doi.org/10.1007/s00158-018-1994-3.

[9] D. Bhate, C. Penick, L. Ferry, C. Lee, Classification and Selection of Cellular Materials in Mechanical Design: Engineering and Biomimetic Approaches, MDPI Des, 2019 1–27.

[10] T. DebRoy, T. Mukherjee, J.O. Milewski, J.W. Elmer, B. Ribic, J.J. Blecher, W. Zhang, Scientific, technological and economic issues in metal printing and their solutions, Nat. Mater. (2019) 1, https://doi.org/10.1038/s41563-019-0408-2.

[11] T. Wohlers, T. Caffrey, R.I. Campbell, O. Diegel, J. Kowen, Wohlers Report 2018: 3D Printing and Additive Manufacturing State of the Industry, 2018.

[12] A. Thompson, D. McNally, I. Maskery, R.K. Leach, X-ray computed tomography and additive manufacturing in medicine: a review, Int. J. Metrol. Qual. Eng. 8 (2017) 17, https://doi.org/10.1051/ijmqe/2017015.

[13] M. Lowther, S. Louth, A. Davey, A. Hussain, P. Ginestra, L. Carter, N. Eisenstein, L. Grover, S. Cox, Clinical, industrial, and research perspectives on powder bed fusion additively manufactured metal implants, Addit. Manuf. 28 (2019) 565–584, https://doi.org/10.1016/J.ADDMA.2019.05.033.

[14] D. Böckin, A.-M. Tillman, Environmental assessment of additive manufacturing in the automotive industry, J. Clean. Prod. 226 (2019) 977–987, https://doi.org/10.1016/J.JCLEPRO.2019.04.086.

[15] Y.L. Yap, W.Y. Yeong, Additive manufacture of fashion and jewellery products: a mini review, Virtual Phys. Prototyp. 9 (2014) 195–201, https://doi.org/10.1080/17452759.2014.938993.

[16] B. Nagarajan, Z. Hu, X. Song, W. Zhai, J. Wei, Development of micro selective laser melting: the state of the art and future perspectives, Engineering (2019) https://doi.org/10.1016/J.ENG.2019.07.002.

[17] D. Jafari, W.W. Wits, The utilization of selective laser melting technology on heat transfer devices for thermal energy conversion applications: a review, Renew. Sust. Energ. Rev. 91 (2018) 420–442, https://doi.org/10.1016/J.RSER.2018.03.109.

[18] P. Krakhmalev, I. Yadroitsev, I. Yadroitsava, O. de Smidt, P. Krakhmalev, I. Yadroitsev, I. Yadroitsava, O. De Smidt, Functionalization of biomedical Ti6Al4V via in situ alloying by Cu during laser powder bed fusion manufacturing, Materials (Basel) 10 (2017), 1154. https://doi.org/10.3390/ma10101154.

[19] P. Krakhmalev, I. Yadroitsev, Microstructure and properties of intermetallic composite coatings fabricated by selective laser melting of Ti–SiC powder mixtures, Intermetallics 46 (2014) 147–155, https://doi.org/10.1016/J.INTERMET.2013.11.012.

[20] W.H. Yu, S.L. Sing, C.K. Chua, C.N. Kuo, X.L. Tian, Particle-reinforced metal matrix nanocomposites fabricated by selective laser melting: a state of the art review, Prog. Mater. Sci. 104 (2019) 330–379, https://doi.org/10.1016/J.PMATSCI.2019.04.006.

[21] A.A. Zadpoor, Mechanical performance of additively manufactured meta-biomaterials, Acta Biomater. 85 (2019) 41–59, https://doi.org/10.1016/J.ACTBIO.2018.12.038.

[22] J. Van Humbeeck, Shape memory alloys, in: M. Schwartz (Ed.), Smart Mater, CRC Press, Boca Raton, FL, USA, 2009.

[23] Z. Khoo, Y. Liu, J. An, C. Chua, Y. Shen, C. Kuo, Z.X. Khoo, Y. Liu, J. An, C.K. Chua, Y.F. Shen, C.N. Kuo, A review of selective laser melted NiTi shape memory alloy, Materials (Basel) 11 (2018) 519, https://doi.org/10.3390/ma11040519.

[24] A. Mitchell, U. Lafont, M. Hołyńska, C. Semprimoschnig, Additive manufacturing — a review of 4D printing and future applications, Addit. Manuf. 24 (2018) 606–626, https://doi.org/10.1016/J.ADDMA.2018.10.038.

[25] L. De Chiffre, S. Carmignato, J.-P. Kruth, R. Schmitt, A. Weckenmann, Industrial applications of computed tomography, CIRP Ann. - Manuf. Technol. 63 (2014) 655–677, https://doi.org/10.1016/j.cirp.2014.05.011.

[26] E. Maire, P.J. Withers, Quantitative X-ray tomography, Int. Mater. Rev. 59 (2014) 1–43, https://doi.org/10.1179/1743280413Y.0000000023.

[27] M.A. Vicente, J. Minguez, D.C. Gonzalez, The use of computed tomography to explore the microstructure of materials in civil engineering: from rocks to concrete, Comput. Tomogr. - Adv. Appl, InTech, 2017https://doi.org/10.5772/intechopen.69245.

[28] J.P. Kruth, M. Bartscher, S. Carmignato, R. Schmitt, L. De Chiffre, A. Weckenmann, Computed tomography for dimensional metrology, CIRP Ann. - Manuf. Technol. 60 (2011) 821–842, https://doi.org/10.1016/j.cirp.2011.05.006.

[29] A. du Plessis, I. Yadroitsev, I. Yadroitsava, S.G. Le Roux, X-ray microcomputed tomography in additive manufacturing: a review of the current technology and applications, 3D Print. Addit. Manuf. 5 (2018) https://doi.org/10.1089/3dp.2018.00603dp.2018.0060.

[30] A. Thompson, I. Maskery, R.K. Leach, X-ray computed tomography for additive manufacturing: a review, Meas. Sci. Technol. 27 (2016) https://doi.org/10.1088/0957-0233/27/7/072001.

[31] S. Romano, A. Abel, J. Gumpinger, A.D. Brandão, S. Beretta, Quality control of AlSi10Mg produced by SLM: metallography versus CT scans for critical defect size assessment, Addit. Manuf. 28 (2019) 394–405, https://doi.org/10.1016/J.ADDMA.2019.05.017.

[32] W.E. King, H.D. Barth, V.M. Castillo, G.F. Gallegos, J.W. Gibbs, D.E. Hahn, C. Kamath, A.M. Rubenchik, Observation of keyhole-mode laser melting in laser powder-bed fusion additive manufacturing, J. Mater. Process. Technol. 214 (2014) 2915–2925, https://doi.org/10.1016/J.JMATPROTEC.2014.06.005.

[33] S.A. Khairallah, A.T. Anderson, A. Rubenchik, W.E. King, Laser powder-bed fusion additive manufacturing: physics of complex melt flow and formation mechanisms of pores, spatter, and denudation zones, Acta Mater. 108 (2016) 36–45, https://doi.org/10.1016/J.ACTAMAT.2016.02.014.

[34] M. Tang, P.C. Pistorius, J.L. Beuth, Prediction of lack-of-fusion porosity for powder bed fusion, Addit. Manuf. 14 (2017) 39–48, https://doi.org/10.1016/J.ADDMA.2016.12.001.

[35] A. Du Plessis, S.G. Le Roux, G. Booysen, J. Els, Directionality of cavities and porosity formation in powder-bed laser additive manufacturing of metal components investigated using X-ray tomography, 3D Print. Addit. Manuf. 3 (2016) https://doi.org/10.1089/3dp.2015.0034.

[36] H. Gong, K. Rafi, H. Gu, T. Starr, B. Stucker, Analysis of defect generation in Ti-6Al-4V parts made using powder bed fusion additive manufacturing processes, Addit. Manuf. 1 (2014) 87–98, https://doi.org/10.1016/j.addma.2014.08.002.

[37] A. du Plessis, S.G. le Roux, Standardized X-ray tomography testing of additively manufactured parts: a round robin test, Addit. Manuf. 24 (2018) 125–136, https://doi.org/10.1016/j.addma.2018.09.014.

[38] J.A. Slotwinski, E.J. Garboczi, K.M. Hebenstreit, Porosity measurements and analysis for metal additive manufacturing process control, J. Res. Natl. Inst. Stand. Technol. 119 (2014) 494–528, https://doi.org/10.6028/jres.119.019.

[39] B. Dutton, W. Vesga, J. Waller, S. James, M. Seifi, in: M. Seifi, N. Shamsaei (Eds.), Metal Additive Manufacturing Defect Formation and Non-Destructive Evaluation (NDE) Detectability, 2018 , ASTM STP 1620.

[40] A. Hilaire, E. Andrieu, X. Wu, High-temperature mechanical properties of alloy 718 produced by laser powder bed fusion with different processing parameters, Addit. Manuf. 26 (2019) 147–160, https://doi.org/10.1016/j.addma.2019.01.012.

[41] W.E. Frazier, Metal additive manufacturing: a review, J. Mater. Eng. Perform. 23 (2014) 1917–1928, https://doi.org/10.1007/s11665-014-0958-z.

[42] C. Zitelli, P. Folgarait, A. Di Di Schino, C. Zitelli, P. Folgarait, A. Di Schino, Laser powder bed fusion of stainless steel grades: a review, Metals (Basel) 9 (2019) 731, https://doi.org/10.3390/met9070731.

[43] J.J. Lewandowski, M. Seifi, Metal additive manufacturing: a review of mechanical properties, Annu. Rev. Mater. Res. 46 (2016) 151–186, https://doi.org/10.1146/annurev-matsci-070115-032024.

[44] R. Morgan, C.J. Sutcliffe, W. O'Neill, Density analysis of direct metal laser re-melted 316L stainless steel cubic primitives, J. Mater. Sci. 39 (2004) 1195–1205, https://doi.org/10.1023/B:JMSC.0000013875.62536.fa.

[45] S. Coeck, M. Bisht, J. Plas, F. Verbist, Prediction of lack of fusion porosity in selective laser melting based on melt pool monitoring data, Addit. Manuf. 25 (2019) 347–356, https://doi.org/10.1016/J.ADDMA.2018.11.015.

[46] P. Krakhmalev, G. Fredriksson, I. Yadroitsava, N. Kazantseva, A. du Plessis, I. Yadroitsev, Deformation behavior and microstructure of Ti6Al4V manufactured by SLM, Phys. Procedia 83 (2016) 778–788, https://doi.org/10.1016/J.PHPRO.2016.08.080.

[47] I. Yadroitsev, P. Krakhmalev, I. Yadroitsava, Hierarchical design principles of selective laser melting for high quality metallic objects, Addit. Manuf. 7 (2015) 45–56, https://doi.org/10.1016/J.ADDMA.2014.12.007.

[48] S. Tammas-Williams, P.J. Withers, I. Todd, P.B. Prangnell, The effectiveness of hot isostatic pressing for closing porosity in titanium parts manufactured by selective electron beam melting, Metall. Mater. Trans. A Phys. Metall. Mater. Sci. 47 (2016) 1939–1946, https://doi.org/10.1007/s11661-016-3429-3.

[49] S. Tammas-Williams, P.J. Withers, I. Todd, P.B. Prangnell, Porosity regrowth during heat treatment of hot isostatically pressed additively manufactured titanium components, Scr. Mater. 122 (2016) 72–76, https://doi.org/10.1016/J.SCRIPTAMAT.2016.05.002.

[50] C.B. Finfrock, A. Exil, J.D. Carroll, L. Deibler, Effect of hot Isostatic pressing and powder feedstock on porosity, microstructure, and mechanical properties of selective laser melted AlSi10Mg, Metallogr. Microstruct. Anal. 7 (2018) 443–456, https://doi.org/10.1007/s13632-018-0456-z.

[51] W. Schneller, M. Leitner, S. Springer, F. Grün, M. Taschauer, W. Schneller, M. Leitner, S. Springer, F. Grün, M. Taschauer, Effect of HIP treatment on microstructure and fatigue strength of selectively laser melted AlSi10Mg, J. Manuf. Mater. Process. 3 (2019) 16, https://doi.org/10.3390/jmmp3010016.

[52] B. Zhou, J. Zhou, H. Li, F. Lin, A study of the microstructures and mechanical properties of Ti6Al4V fabricated by SLM under vacuum, Mater. Sci. Eng. A 724 (2018) 1–10, https://doi.org/10.1016/J.MSEA.2018.03.021.

[53] C.N. Kelly, N.T. Evans, C.W. Irvin, S.C. Chapman, K. Gall, D.L. Safranski, The effect of surface topography and porosity on the tensile fatigue of 3D printed Ti-6Al-4V fabricated by selective laser melting, Mater. Sci. Eng. C. 98 (2019) 726–736, https://doi.org/10.1016/J.MSEC.2019.01.024.

[54] J.K. Chen, M.W. Wu, T.L. Cheng, P.H. Chiang, Continuous compression behaviors of selective laser melting Ti-6Al-4V alloy with cuboctahedron cellular structures, Mater. Sci. Eng. C. 100 (2019) 781–788, https://doi.org/10.1016/J.MSEC.2019.03.054.

[55] M. Seifi, M. Gorelik, J. Waller, N. Hrabe, N. Shamsaei, S. Daniewicz, J.J. Lewandowski, Progress towards metal additive manufacturing standardization to support qualification and certification, JOM 69 (2017) 439–455, https://doi.org/10.1007/s11837-017-2265-2.

[56] M. Seifi, A. Salem, J. Beuth, O. Harrysson, J.J. Lewandowski, Overview of materials qualification needs for metal additive manufacturing, JOM 68 (2016) 747–764, https://doi.org/10.1007/s11837-015-1810-0.

[57] R. Rashid, S.H. Masood, D. Ruan, S. Palanisamy, R.A. Rahman Rashid, M. Brandt, Effect of scan strategy on density and metallurgical properties of 17-4PH parts printed by Selective Laser Melting (SLM), J. Mater. Process. Technol. 249 (2017) 502–511, https://doi.org/10.1016/J.JMATPROTEC.2017.06.023.

[58] T. Zikmund, J. Šalplachta, A. Zatočilová, A. Břínek, L. Pantělejev, R. Štěpánek, D. Koutný, D. Paloušek, J. Kaiser, Computed tomography based procedure for reproducible porosity measurement of additive manufactured samples, NDT E Int 103 (2019) 111–118, https://doi.org/10.1016/J.NDTEINT.2019.02.008.

[59] ASTM International, ASTM F3001-14: Standard Specification for Additive Manufacturing Titanium-6 Aluminum-4 Vanadium ELI (Extra Low Interstitial) With Powder Bed Fusion, i, 2012 1–8, https://doi.org/10.1520/F2924-12A.2.

[60] I. Yadroitsev, P. Krakhmalev, I. Yadroitsava, A. Du Plessis, Qualification of Ti6Al4V ELI alloy produced by laser powder bed fusion for biomedical applications, JOM 70 (2018) 372–377, https://doi.org/10.1007/s11837-017-2655-5.

[61] I. van Zyl, I. Yadroitsava, I. Yadroitsev, I. Yadroitsev, Residual stress in Ti6Al4V objects produced by direct metal laser sintering, South African J. Ind. Eng. 27 (2016) 134–141, https://doi.org/10.7166/27-4-1468.

[62] I. Yadroitsava, I. Yadroitsev, Residual stress in metal specimens produced by direct metal laser sintering, Solid Free. Fabr. Symp 2015, pp. 10–12. http://sffsymposium.engr.utexas.edu/sites/default/files/2015/2015-49-Yadroitsev.pdf.

[63] Y.Y. Sun, S. Gulizia, C.H. Oh, D. Fraser, M. Leary, Y.F. Yang, M. Qian, The influence of as-built surface conditions on mechanical properties of Ti-6Al-4V additively manufactured by selective electron beam melting, JOM 68 (2016) 791–798, https://doi.org/10.1007/s11837-015-1768-y.

[64] A. du Plessis, P. Sperling, A. Beerlink, O. Kruger, L. Tshabalala, S. Hoosain, S.G. le Roux, Standard method for microCT-based additive manufacturing quality control 3: surface roughness, MethodsX 5 (2018) 1111–1116, https://doi.org/10.1016/j.mex.2018.09.006.

[65] U. Zerbst, K. Hilgenberg, Damage development and damage tolerance of structures manufactured by selective laser melting – a review, Procedia Struct. Integr. 7 (2017) 141–148, https://doi.org/10.1016/j.prostr.2017.11.071.

[66] V. Cnudde, M.N. Boone, High-resolution X-ray computed tomography in geosciences: a review of the current technology and applications, Earth-Science Rev 123 (2013) 1–17, https://doi.org/10.1016/j.earscirev.2013.04.003.

[67] A. du Plessis, W.P. Boshoff, A review of X-ray computed tomography of concrete and asphalt construction materials, Constr. Build. Mater. 199 (2019) 637–651, https://doi.org/10.1016/j.conbuildmat.2018.12.049.

[68] L. Schoeman, P. Williams, A. du Plessis, M. Manley, X-ray micro-computed tomography (μCT) for non-destructive characterisation of food microstructure, Trends Food Sci. Technol. (2016) https://doi.org/10.1016/j.tifs.2015.10.016.

[69] A. du Plessis, C. Broeckhoven, Looking deep into nature: a review of micro-computed tomography in biomimicry, Acta Biomater. 85 (2019) 27–40, https://doi.org/10.1016/j.actbio.2018.12.014.

[70] C. Broeckhoven, A. du Plessis, X-ray microtomography in herpetological research: a review, Amphibia-Reptilia 39 (2018) 377–401.

[71] A. du Plessis, C. Broeckhoven, A. Guelpa, S.G. le Roux, Laboratory x-ray micro-computed tomography: a user guideline for biological samples, Gigascience 6 (2017) 42–49, https://doi.org/10.1093/gigascience/gix027.

[72] A. du Plessis, S.G. le Roux, M. Tshibalanganda, Advancing X-ray micro computed tomography in Africa: going far, together, Sci. African. 3 (2019) e00061, https://doi.org/10.1016/j.sciaf.2019.e00061.

[73] H. Villarraga-Gómez, C. Lee, S.T. Smith, Dimensional metrology with X-ray CT: a comparison with CMM measurements on internal features and compliant structures, Precis. Eng. 51 (2018) 291–307, https://doi.org/10.1016/J.PRECISIONENG.2017.08.021.

[74] A. du Plessis, P. Sperling, A. Beerlink, L. Tshabalala, S. Hoosain, N. Mathe, S.G. le Roux, Standard method for microCT-based additive manufacturing quality control 1: Porosity analysis. MethodsX, 5, 2018 1102–1110 Vancouver.

[75] A. du Plessis, P. Sperling, A. Beerlink, L. Tshabalala, S. Hoosain, N. Mathe, G. Stephan, MethodsX standard method for microCT-based additive manufacturing quality control 2: density measurement, MethodsX 5 (2018) 1117–1123, https://doi.org/10.1016/j.mex.2018.09.006.

[76] A. du Plessis, P. Sperling, A. Beerlink, W. du Preez, S.G. le Roux, Standard method for microCT-based additive manufacturing quality control 4: metal powder analysis, MethodsX 5 (2018) 1336–1345, https://doi.org/10.1016/j.mex.2018.09.006.

[77] A.A. Martin, N.P. Calta, S.A. Khairallah, J. Wang, P.J. Depond, A.Y. Fong, V. Thampy, G.M. Guss, A.M. Kiss, K.H. Stone, C.J. Tassone, J. Nelson Weker, M.F. Toney, T. van Buuren, M.J. Matthews, Dynamics of pore formation during laser powder bed fusion additive manufacturing, Nat. Commun. 10 (2019) 1–10, https://doi.org/10.1038/s41467-019-10009-2.

[78] D. Manfredi, F. Calignano, M. Krishnan, R. Canali, E. Paola, S. Biamino, D. Ugues, M. Pavese, P. Fino, Additive manufacturing of Al alloys and aluminium matrix composites (AMCs), Light Met. Alloy. Appl, InTech, 2014https://doi.org/10.5772/58534.

[79] B. Wysocki, P. Maj, A. Krawczyńska, K. Rożniatowski, J. Zdunek, K.J. Kurzydłowski, W. Święszkowski, Microstructure and mechanical properties investigation of CP titanium processed by selective laser melting (SLM), J. Mater. Process. Technol. 241 (2017) 13–23, https://doi.org/10.1016/J.JMATPROTEC.2016.10.022.

[80] H. Choo, K.-L. Sham, J. Bohling, A. Ngo, X. Xiao, Y. Ren, P.J. Depond, M.J. Matthews, E. Garlea, Effect of laser power on defect, texture, and microstructure of a laser powder bed fusion processed 316L stainless steel, Mater. Des. 164 (2019), 107534. https://doi.org/10.1016/J.MATDES.2018.12.006.

[81] S. Tammas-Williams, H. Zhao, F. Léonard, F. Derguti, I. Todd, P.B. Prangnell, XCT analysis of the influence of melt strategies on defect population in Ti–6Al–4V components manufactured by Selective Electron Beam Melting, Mater. Charact. 102 (2015) 47–61, https://doi.org/10.1016/J.MATCHAR.2015.02.008.

[82] I. Watanabe, J.H. Watkins, H. Nakajima, M. Atsuta, T. Okabe, Effect of pressure difference on the quality of titanium casting, J. Dent. Res. 76 (1997) 773–779, https://doi.org/10.1177/00220345970760031001.

[83] A. du Plessis, I. Yadroitsava, S.G. le Roux, I. Yadroitsev, J. Fieres, C. Reinhart, P. Rossouw, Prediction of mechanical performance of Ti6Al4V cast alloy based on microCT-based load simulation, J. Alloys Compd. 724 (2017) 267–274, https://doi.org/10.1016/J.JALLCOM.2017.06.320.

[84] J.F. Magland, N. Zhang, C.S. Rajapakse, F.W. Wehrli, Computationally-optimized bone mechanical modeling from high-resolution structural images, PLoS One 7 (2012), e35525. https://doi.org/10.1371/journal.pone.0035525.

[85] C.A. Kantzos, R.W. Cunningham, V. Tari, A.D. Rollett, Characterization of metal additive manufacturing surfaces using synchrotron X-ray CT and micromechanical

modeling, Comput. Mech. 61 (2018) 575–580, https://doi.org/10.1007/s00466-017-1531-z.
[86] A. Arshadi, H. Bahia, Development of an image-based multi-scale finite-element approach to predict mechanical response of asphalt mixtures, Road Mater. Pavement Des. 16 (2015) 214–229, https://doi.org/10.1080/14680629.2015.1077007.
[87] W. Huang, X. Zhang, Y. Yin, An image-based finite element approach for simulating viscoelastic response of asphalt mixture, Adv. Mater. Sci. Eng. 2016 (2016) 1–11, https://doi.org/10.1155/2016/7428623.
[88] ASTM WK56649, Standard Practice/Guide for Intentionally Seeding Flaws in Additively Manufactured (AM) Parts, 2018.
[89] A.E. Wilson-Heid, T.C. Novak, A.M. Beese, Characterization of the effects of internal pores on tensile properties of additively manufactured austenitic stainless steel 316L, Exp. Mech. (2018) https://doi.org/10.1007/s11340-018-00465-0.
[90] D. Kouprianoff, A.D. Plessis, I. Yadroitsava, I. Yadroitsev, Non-destructive testing of the parts manufactured by direct metal laser sintering, Proc. 18th Int. Conf. RAPDASA, 7–10 Novemb. 2017, Durban ICC, South Africa, 2017.
[91] T. Mishurova, K. Artzt, J. Haubrich, G. Requena, G. Bruno, New aspects about the search for the most relevant parameters optimizing SLM materials, Addit. Manuf. 25 (2019) 325–334, https://doi.org/10.1016/J.ADDMA.2018.11.023.
[92] H. Gong, K. Rafi, H. Gu, G.D. Janaki Ram, T. Starr, B. Stucker, Influence of defects on mechanical properties of Ti–6Al–4 V components produced by selective laser melting and electron beam melting, Mater. Des. 86 (2015) 545–554, https://doi.org/10.1016/J.MATDES.2015.07.147.
[93] J. Stef, A. Poulon-Quintin, A. Redjaïmia, J. Ghanbaja, O. Ferry, M. De Sousa, M. Gouné, Mechanism of porosity formation and influence on mechanical properties in selective laser melting of Ti-6Al-4V parts, Mater. Des. 156 (2018) 480–493, https://doi.org/10.1016/j.matdes.2018.06.049ï.
[94] J. Elambasseril, S.L. Lu, Y.P. Ning, N. Liu, J. Wang, M. Brandt, H.P. Tang, M. Qian, 3D characterization of defects in deep-powder-bed manufactured Ti–6Al–4V and their influence on tensile properties, Mater. Sci. Eng. A 761 (2019), 138031. https://doi.org/10.1016/J.MSEA.2019.138031.
[95] T. Voisin, N.P. Calta, S.A. Khairallah, J.-B. Forien, L. Balogh, R.W. Cunningham, A.D. Rollett, Y.M. Wang, Defects-dictated tensile properties of selective laser melted Ti-6Al-4V, Mater. Des. 158 (2018) 113–126, https://doi.org/10.1016/J.MATDES.2018.08.004.
[96] M. Salarian, H. Asgari, M. Vlasea, Pore space characteristics and corresponding effect on tensile properties of Inconel 625 fabricated via laser powder bed fusion, Mater. Sci. Eng. A 769 (2020) https://doi.org/10.1016/j.msea.2019.138525.
[97] H.D. Carlton, A. Haboub, G.F. Gallegos, D.Y. Parkinson, A.A. Mac Dowell, Damage evolution and failure mechanisms in additively manufactured stainless steel, Mater. Sci. Eng. A 651 (2016) 406–414, https://doi.org/10.1016/j.msea.2015.10.073.
[98] C. Pei, D. Shi, H. Yuan, H. Li, Assessment of mechanical properties and fatigue performance of a selective laser melted nickel-base superalloy Inconel 718, Mater. Sci. Eng. A 759 (2019) 278–287, https://doi.org/10.1016/J.MSEA.2019.05.007.
[99] J. Elambasseril, S.L. Lu, Y.P. Ning, N. Liu, J. Wang, M. Brandt, H.P. Tang, M. Qian, 3D characterization of defects in deep-powder-bed manufactured Ti–6Al–4V and their influence on tensile properties, Mater. Sci. Eng. A (2019) 138031, https://doi.org/10.1016/j.msea.2019.138031.
[100] U. Zerbst, M. Madia, C. Klinger, D. Bettge, Y. Murakami, Defects as a root cause of fatigue failure of metallic components. I: basic aspects, Eng. Fail. Anal. 97 (2019) 777–792, https://doi.org/10.1016/j.engfailanal.2019.01.055.
[101] U. Zerbst, M. Madia, C. Klinger, D. Bettge, Y. Murakami, Defects as a root cause of fatigue failure of metallic components. II: non-metallic inclusions, Eng. Fail. Anal. (2019) 1–12, https://doi.org/10.1016/j.engfailanal.2019.01.054.
[102] Y. Murakami, C. Klinger, M. Madia, U. Zerbst, D. Bettge, Defects as a root cause of fatigue failure of metallic components. III: cavities, dents, corrosion pits, scratches, Eng. Fail. Anal. 97 (2019) 759–776, https://doi.org/10.1016/j.engfailanal.2019.01.034.
[103] Y. Murakami, Metal Fatigue: Effects of Small Defects and Nonmetallic Inclusions, Elsevier, 2002.
[104] A.D. Brandão, J. Gumpinger, M. Gschweitl, C. Seyfert, P. Hofbauer, T. Ghidini, Fatigue properties of additively manufactured AlSi10Mg-surface treatment effect, Procedia Struct. Integr. 7 (2017) 58–66, https://doi.org/10.1016/j.prostr.2017.11.061.
[105] M. Tang, P.C. Pistorius, Fatigue life prediction for AlSi10Mg components produced by selective laser melting, Int. J. Fatigue 125 (2019) 479–490, https://doi.org/10.1016/J.IJFATIGUE.2019.04.015.
[106] N.O. Larrosa, W. Wang, N. Read, M.H. Loretto, C. Evans, J. Carr, U. Tradowsky, M.M. Attallah, P.J. Withers, Linking microstructure and processing defects to mechanical properties of selectively laser melted AlSi10Mg alloy, Theor. Appl. Fract. Mech. 98 (2018) 123–133, https://doi.org/10.1016/J.TAFMEC.2018.09.011.
[107] J. Zhao, M. Easton, M. Qian, M. Leary, M. Brandt, Effect of building direction on porosity and fatigue life of selective laser melted AlSi12Mg alloy, Mater. Sci. Eng. A 729 (2018) 76–85, https://doi.org/10.1016/J.MSEA.2018.05.040.
[108] S. Romano, A. Brandão, J. Gumpinger, M. Gschweitl, S. Beretta, Qualification of AM parts: extreme value statistics applied to tomographic measurements, Mater. Des. 131 (2017) 32–48, https://doi.org/10.1016/J.MATDES.2017.05.091.
[109] Q.C. Liu, J. Elambasseril, S.J. Sun, M. Leary, M. Brandt, P.K. Sharp, The effect of manufacturing defects on the fatigue behaviour of Ti-6Al-4V specimens fabricated using selective laser melting, Adv. Mater. Res, , Trans Tech Publications, 2014 1519–1524, https://doi.org/10.4028/www.scientific.net/AMR.891-892.1519.
[110] L.B. Malefane, W.B. Du Preez, M. Maringa, A. Du Plessis, Tensile and high cycle fatigue properties of annealed Ti6Al4V (ELI) specimens produced by direct metal laser sintering, South African J. Ind. Eng. 29 (2018) 299–311, https://doi.org/10.7166/29-3-2077.
[111] O. Andreau, E. Pessard, I. Koutiri, J.D. Penot, C. Dupuy, N. Saintier, P. Peyre, A competition between the contour and hatching zones on the high cycle fatigue behaviour of a 316L stainless steel: analyzed using X-ray computed tomography, Mater. Sci. Eng. A 757 (2019) 146–159, https://doi.org/10.1016/j.msea.2019.04.101.
[112] M. Benedetti, V. Fontanari, M. Bandini, F. Zanini, S. Carmignato, Low- and high-cycle fatigue resistance of Ti-6Al-4V ELI additively manufactured via selective laser melting: mean stress and defect sensitivity, Int. J. Fatigue 107 (2018) 96–109, https://doi.org/10.1016/J.IJFATIGUE.2017.10.021.
[113] R. Shrestha, J. Simsiriwong, N. Shamsaei, Fatigue behavior of additive manufactured 316L stainless steel parts: effects of layer orientation and surface roughness, Addit. Manuf. 28 (2019) 23–38, https://doi.org/10.1016/j.addma.2019.04.011.
[114] S. Tammas-Williams, P.J. Withers, I. Todd, P.B. Prangnell, The influence of porosity on fatigue crack initiation in additively manufactured titanium components, Sci. Rep. 7 (2017) 7308, https://doi.org/10.1038/s41598-017-06504-5.
[115] H.V. Atkinson, S. Davies, Fundamental aspects of hot isostatic pressing: an overview, Metall. Mater. Trans. A Phys. Metall. Mater. Sci. 31 (2000) 2981–3000, https://doi.org/10.1007/s11661-000-0078-2.
[116] E. Uhlmann, R. Kersting, T.B. Klein, M.F. Cruz, A.V. Borille, Additive manufacturing of titanium alloy for aircraft components, Procedia CIRP 35 (2015) 55–60, https://doi.org/10.1016/j.procir.2015.08.061.
[117] J. Damon, S. Dietrich, F. Vollert, J. Gibmeier, V. Schulze, Process dependent porosity and the influence of shot peening on porosity morphology regarding selective laser melted AlSi10Mg parts, Addit. Manuf. 20 (2018) 77–89, https://doi.org/10.1016/J.ADDMA.2018.01.001.
[118] N.E. Uzan, S. Ramati, R. Shneck, N. Frage, O. Yeheskel, On the effect of shot-peening on fatigue resistance of AlSi10Mg specimens fabricated by additive manufacturing using selective laser melting (AM-SLM), Addit. Manuf. 21 (2018) 458–464, https://doi.org/10.1016/j.addma.2018.03.030.
[119] L. Hackel, J.R. Rankin, A. Rubenchik, W.E. King, M. Matthews, Laser peening: a tool for additive manufacturing post-processing, Addit. Manuf. 24 (2018) 67–75, https://doi.org/10.1016/j.addma.2018.09.013.
[120] A. du Plessis, D. Glaser, H. Moller, N. Mathe, L. Tshabalala, B. Mfusi, R. Mostert, Pore closure effect of laser shock peening of additively manufactured AlSi10Mg, 3D Print. Addit. Manuf. 6 (2019) https://doi.org/10.1089/3dp.2019.0064.
[121] R. Cunningham, C. Zhao, N. Parab, C. Kantzos, J. Pauza, K. Fezzaa, T. Sun, A.D. Rollett, Keyhole threshold and morphology in laser melting revealed by ultrahigh-speed x-ray imaging, Science (80-.) 363 (2019) 849–852, https://doi.org/10.1126/science.aav4687.
[122] C.L.A. Leung, S. Marussi, R.C. Atwood, M. Towrie, P.J. Withers, P.D. Lee, In situ X-ray imaging of defect and molten pool dynamics in laser additive manufacturing, Nat. Commun. 9 (2018) 1–9, https://doi.org/10.1038/s41467-018-03734-7.
[123] C. Zhao, K. Fezzaa, R.W. Cunningham, H. Wen, F. De Carlo, L. Chen, A.D. Rollett, T. Sun, Real-time monitoring of laser powder bed fusion process using high-speed X-ray imaging and diffraction, Sci. Rep. 7 (2017) 1–11, https://doi.org/10.1038/s41598-017-03761-2.
[124] A. du Plessis, Effects of process parameters on porosity in laser powder bed fusion revealed by X-ray tomography, Addit. Manuf. 30 (2019) 100871.
[125] N. Sanaei, A. Fatemi, N. Phan, Defect characteristics and analysis of their variability in metal L-PBF additive manufacturing, Mater. Des. 182 (2019), 108091. https://doi.org/10.1016/j.matdes.2019.108091.
[126] A.D. Plessis, S.G. Le Roux, G. Booysen, J. Els, Quality control of a laser additive manufactured medical implant by X-ray tomography, 3D Print, Addit. Manuf. 3 (2016) 175–182, https://doi.org/10.1089/3dp.2016.0012.
[127] J. Fieres, P. Schumann, C. Reinhart, Predicting failure in additively manufactured parts using X-ray computed tomography and simulation, Procedia Eng 213 (2018) 69–78, https://doi.org/10.1016/J.PROENG.2018.02.008.
[128] A. du Plessis, I. Yadroitsava, D.-P. Kouprianoff, I. Yadroitsev, Numerical and experimental study of the effect of artificial porosity in a lattice structure manufactured by laser based powder, Solid Free. Fabr. Symp, 2018.
[129] P. Foteinopoulos, A. Papacharalampopoulos, P. Stavropoulos, On thermal modeling of additive manufacturing processes, CIRP J. Manuf. Sci. Technol. 20 (2018) 66–83, https://doi.org/10.1016/J.CIRPJ.2017.09.007.
[130] H. Peng, D.B. Go, R. Billo, S. Gong, M.R. Shankar, B.A. Gatrell, J. Budzinski, P. Ostiguy, R. Attardo, C. Tomonto, J. Neidig, D. Hoelzle, Part-scale model for fast prediction of thermal distortion in DMLS additive manufacturing; part 2: a quasi-static thermomechanical model, Proc. 27th Annu. Int. Solid Free. Fabr. Symp 2016, pp. 361–381.
[131] K. Bartsch, F. Lange, M. Gralow, C. Emmelmann, Novel approach to optimized support structures in laser beam melting by combining process simulation with topology optimization, J. Laser Appl. 31 (2019), 022302. https://doi.org/10.2351/1.5096096.
[132] W. King, A.T. Anderson, R.M. Ferencz, N.E. Hodge, C. Kamath, S.A. Khairallah, Overview of modelling and simulation of metal powder bed fusion process at Lawrence Livermore National Laboratory, Mater. Sci. Technol. 31 (2015) 957–968, https://doi.org/10.1179/1743284714Y.0000000728.
[133] R. Biswal, A.K. Syed, X. Zhang, Assessment of the effect of isolated porosity defects on the fatigue performance of additive manufactured titanium alloy, Addit. Manuf. 23 (2018) 433–442, https://doi.org/10.1016/J.ADDMA.2018.08.024.
[134] A. du Plessis, I. Yadroitsava, I. Yadroitsev, S. le Roux, D. Blaine, Numerical comparison of lattice unit cell designs for medical implants by additive manufacturing, Virtual Phys. Prototyp. (2018) 1–16, https://doi.org/10.1080/17452759.2018.1491713.
[135] A. du Plessis, I. Yadroitsava, I. Yadroitsev, Ti6Al4V lightweight lattice structures manufactured by laser powder bed fusion for load-bearing applications, Opt. Laser Technol. (2018) https://doi.org/10.1016/j.optlastec.2018.07.050.

[136] M. Dallago, B. Winiarski, F. Zanini, S. Carmignato, M. Benedetti, On the effect of geometrical imperfections and defects on the fatigue strength of cellular lattice structures additively manufactured via Selective Laser Melting, Int. J. Fatigue 124 (2019) 348–360, https://doi.org/10.1016/J.IJFATIGUE.2019.03.019.
[137] M. Hamidi Nasab, S. Romano, D. Gastaldi, S. Beretta, M. Vedani, Combined effect of surface anomalies and volumetric defects on fatigue assessment of AlSi7Mg fabricated via laser powder bed fusion, Addit. Manuf. (2019), 100918. https://doi.org/10.1016/j.addma.2019.100918.
[138] A.M. Vilardell, G. Fredriksson, I. Yadroitsev, P. Krakhmalev, Fracture mechanisms in the as-built and stress-relieved laser powder bed fusion Ti6Al4V ELI alloy, Opt. Laser Technol. 109 (2019) 608–615, https://doi.org/10.1016/j.optlastec.2018.08.042.